The Canadian Mineralogist
Vol. 34, pp. 1253-1286 (1996)

EMERALD MINERALIZATION AND METASOMATISM OF AMPHIBOLITE, KHALTARO GRANITIC PEGMATITE – HYDROTHERMAL VEIN SYSTEM, HARAMOSH MOUNTAINS, NORTHERN PAKISTAN

BRENDAN M. LAURS[1] AND JOHN H. DILLES[2]

Department of Geosciences, Oregon State University, Corvallis, Oregon 97331, U.S.A.

LAWRENCE W. SNEE[2]

U.S. Geological Survey, Mail Stop 913, Federal Center, Denver, Colorado 80225, U.S.A.

ABSTRACT

Emerald mineralization is found within 0.1- to 1-m-thick hydrothermal veins and granitic pegmatites cutting amphibolite within the Nanga Parbat – Haramosh massif, in northern Pakistan. The amphibolite forms a sill-like body within garnet–mica schist, and both are part of a regional layered gneiss unit of Proterozoic (?) age. The $^{40}Ar/^{39}Ar$ data for muscovite from a pegmatite yield a plateau age of 9.13 ± 0.04 Ma. Muscovite from mica schist and hornblende from amphibolite yield disturbed spectra with interpreted ages of 9 to 10 Ma and more than 225 Ma, respectively, which indicate that peak Tertiary metamorphism reached 325 to 550°C prior to 10 Ma. Pegmatites were emplaced after peak metamorphism during this interval and are older than pegmatites farther south in the massif. At Khaltaro, simply zoned albite-rich miarolitic pegmatites and hydrothermal veins containing various proportions of quartz, albite, tourmaline, muscovite, and beryl are associated with a 1- to 3-m-thick heterogeneous leucogranite sill, that is locally albitized. The pegmatites likely crystallized at 650 to 600°C at pressures of less than 2 kbar. Crystals of emerald form within thin (<30 cm) veins of quartz and tourmaline–albite, and more rarely in pegmatite, near the contacts with altered amphibolite. The emerald-green coloration is produced by Cr and Fe. The Cr and total Fe contents, expressed as Cr_2O_3 and Fe_2O_3, respectively, decrease systematically from emerald (>0.20, 0.54–0.89 wt%), to pale blue beryl (≤0.07, 0.10–0.63%), to colorless beryl (<0.07, 0.07–0.28%). The amphibolite is metasomatized in less than 20-cm-wide selvages that are symmetrically zoned around veins or pegmatites. A sporadic inner zone containing F-rich biotite, tourmaline, and fluorite, with local albite, muscovite, quartz, and rare beryl, gives way to an intermediate zone containing biotite and fluorite with local plagioclase and quartz, and to an outer zone of amphibolite containing sparse biotite and local quartz. The inner and intermediate zones experienced gains of K, H, F, B, Li, Rb, Cs, Be, Ta, Nb, As, Y and Sr, and losses of Si, Mg, Ca, Fe, Cr, V and Sc. The outer alteration zone has gained F, Li, Rb, Cs, and As. Oxygen isotope analyses of igneous and hydrothermal minerals indicate that a single fluid of magmatic origin with $\delta^{18}O_{H_2O} = 8‰$ produced the pegmatite–vein system and hydrothermal alteration at temperatures between 550 and 400°C. The formation of emerald results from introduction of HF-rich magmatic-hydrothermal fluids into the amphibolite, which caused hydrogen ion metasomatism and released Cr and Fe into the pegmatite–vein system.

Keywords: granitic pegmatite, hydrothermal vein, leucogranite, emerald, amphibolite, metasomatism, Khaltaro, Nanga Parbat – Haramosh massif, Pakistan.

SOMMAIRE

Nous avons découvert une minéralisation en émeraude à l'intérieur de veines hydrothermales et pegmatitiques recoupant des amphibolites du massif de Nanga Parbat – Haramosh, dans le nord du Pakistan. L'amphibolite forme un niveau ressemblant à un filon-couche dans un schiste à grenat + mica, et les deux unités lithologiques font partie d'une séquence litée gneissique d'aspect régional et d'âge protérozoïque (?). Les données $^{40}Ar/^{39}Ar$ caractérisant la muscovite d'un échantillon de pegmatite granitique établissent un plateau signifiant un âge de 9.13 ± 0.04 Ma. La muscovite d'un schist micacé et la hornblende d'une amphibolite ont un spectre perturbé, avec des âges interprétés de 9 à 10 Ma et de plus de 225 Ma, respectivement; ces résultats indiquent que le paroxysme du métamorphisme tertiaire a atteint un seuil entre 325 et 550°C avant il y a 10 Ma. La mise en place des pegmatites a eu lieu après cette culmination métamorphique dans cet intervalle de temps, et précède les venues pegmatitiques plus au sud dans le massif. A Khaltaro, les pegmatites miarolitiques zonées simplement et les veines hydrothermales contenant des proportions variables de quartz, albite, tourmaline, muscovite et béryl montrent une

[1] *Permanent address:* 507 Marview Lane, Solana Beach, California 92075, U.S.A.
[2] *E-mail addresses:* dillesj@bcc.orst.edu, lsnee@greenwood.cr.usgs.gov

association avec un filon-couche entre 1 et 3 m en épaisseur de leucogranite hétérogène, qui se trouve albitisé ici et là. Les pegmatites ont cristallisé entre 650 et 600°C à une pression inférieure à 2 kbar. Les cristaux d'émeraude se sont formés dans des veinules (<30 cm) de quartz et de tourmaline + albite et, plus rarement, dans la pegmatite même, près de ses contacts avec l'amphibolite altérée. La coloration vert-émeraude est attribuée à la présence de Cr et de Fe, dont les teneurs, exprimées sous forme de Cr_2O_3 et Fe_2O_3, respectivement, diminuent systématiquement de l'émeraude (>0.20, 0.54–0.89% en poids) au béryl bleu pâle (≤0.07, 0.10–0.63%), et enfin au béryl incolore (<0.20, 0.07–0.28%). L'amphibolite se trouve transformée sur une largeur de 20 cm, dans un liseré de part et d'autre des veines hydrothermales ou des venues de pegmatite. Une zone interne, développée ici et là, contient biotite riche en F, tourmaline, et fluorite, avec accumulation locale en albite, muscovite, quartz et, plus rarement, béryl. Vers la zone intermédiaire, la biotite et la fluorite deviennent plus importantes, avec développement local de plagioclase et quartz. Enfin dans la zone externe de l'amphibolite, la biotite devient plus rare, et la présence du quartz n'est que locale. Les zones interne et intermédiaire ont subi un apport de K, H, F, B, Li, Rb, Cs, Be, Ta, Nb, As, Y, et Sr, et une perte en Si, Mg, Ca, Fe, Cr, V, et Sc. La zone externe a subi un apport de F, Li, Rb, Cs, et As. Une analyse des isotopes de l'oxygène des minéraux ignés et hydrothermaux indique la présence d'une seule phase fluide d'origine magmatique, avec $\delta^{18}O_{H_2O} = 8‰$, qui a formé le système de pegmatites et de veines ainsi que l'altération hydrothermale sur l'intervalle de températures compris entre 550 et 400°C. La formation de l'émeraude résulte de l'introduction de cette phase fluide fluorée, d'origine magmatique-hydrothermale, dans l'amphibolite, ce qui a causé une métasomatose à l'ion hydrogène de l'amphibolite et, par ce fait, une mobilisation du Cr et du Fe dans le système pegmatitique et hydrothermal.

(Traduit par la Rédaction)

Mots-clés: pegmatite granitique, veine hydrothermale, leucogranite, émeraude, amphibolite, métasomatose, Khaltaro, massif de Nanga Parbat – Haramosh, Pakistan.

Introduction

Emerald is rarely found in nature, because its formation typically requires the interaction of fluid derived from highly evolved, Be-enriched rocks with Cr-enriched mafic rocks. Such exceptional geological conditions may take place in suture zones, granite–greenstone terranes, and metashales (Kazmi & Snee 1989), where Be-enriched fluids may be derived from crystallization of granitic pegmatite-forming magmas or may arise as a result of interaction with evolved metamorphic rocks. Suture-zone emerald is mined from several locations in northern Pakistan along the Main Mantle Thrust. In the majority of occurrences in Pakistan, the emerald is hosted by talc–carbonate schist, but Kazmi *et al.* (1989) documented one locality in which the emerald is found in granitic pegmatite.

The Khaltaro emerald deposit is located in the northwestern part of the Nanga Parbat – Haramosh massif (hereafter, Haramosh massif), on the northeastern side of Khaltar valley, about 5 km north of Darchan village, at nearly 4200 m above sea level (Figs. 1, 2). Emerald was discovered there by the Gemstone Corporation of Pakistan in 1985 during a reconnaissance study of gem-bearing pegmatites in the Haramosh region (Kazmi *et al.* 1989). Access to the deposit is hindered by the elevation and rugged terrain. Small-scale mining by the Corporation produced about 600 carats of gem-quality emerald from two prospects (Kazmi *et al.* 1989), but the deposits were abandoned owing to poor accessibility and the pale, fractured nature of the emerald. Local inhabitants occasionally mine small quantities of emerald, as well as aquamarine and fluorite crystals from nearby pegmatites.

Kazmi *et al.* (1985) and Kazmi & O'Donoghue (1990) documented the production of gem- and specimen-quality aquamarine, topaz, tourmaline, fluorite, and a variety of rarer mineral species from several bodies of pegmatite in northern Pakistan. The Khaltaro area was described briefly by Kazmi *et al.* (1989), who were unable to visit the deposit and summarized provisional field notes by Khan & Aziz (1985). Accounts of the location and geology of the mine area in Kazmi *et al.* (1989) differ significantly from ours, which are based on detailed field mapping (Laurs 1995). Bank (1985) noted that well-formed crystals of colorless, milky blue, and emerald green beryl are found with tourmaline and albite at Khaltaro. Mariano (1987a, b) examined emerald and associated minerals from Khaltaro and the Swat district in Pakistan using cathodoluminescence; Khaltaro emerald has also been analyzed by electron microprobe and proton-induced excitation analysis (A.N. Mariano, pers. comm., 1995). Results of chemical analyses of emerald from several Pakistani locations, including Khaltaro, are reported in Snee *et al.* (1989) and Hammarstrom (1989). Madin (1986) documented the structure and tectonics of the northwestern Haramosh massif, and described the high-angle Raikot fault along its western boundary. Butler *et al.* (1992) used binoculars to map the Main Mantle Thrust around the northern margin of the Haramosh massif, and documented the Jutial leucogranite, which lies 3 km southeast of the Khaltaro emerald deposit (Fig. 2).

Emerald deposits associated with granitic pegmatite and hydrothermal veins are the most abundant and widespread type in the world; they are found in Asia (Pakistan, Afghanistan, India, Russia), Africa (Egypt, Tanzania, Mozambique, Madagascar, Zambia,

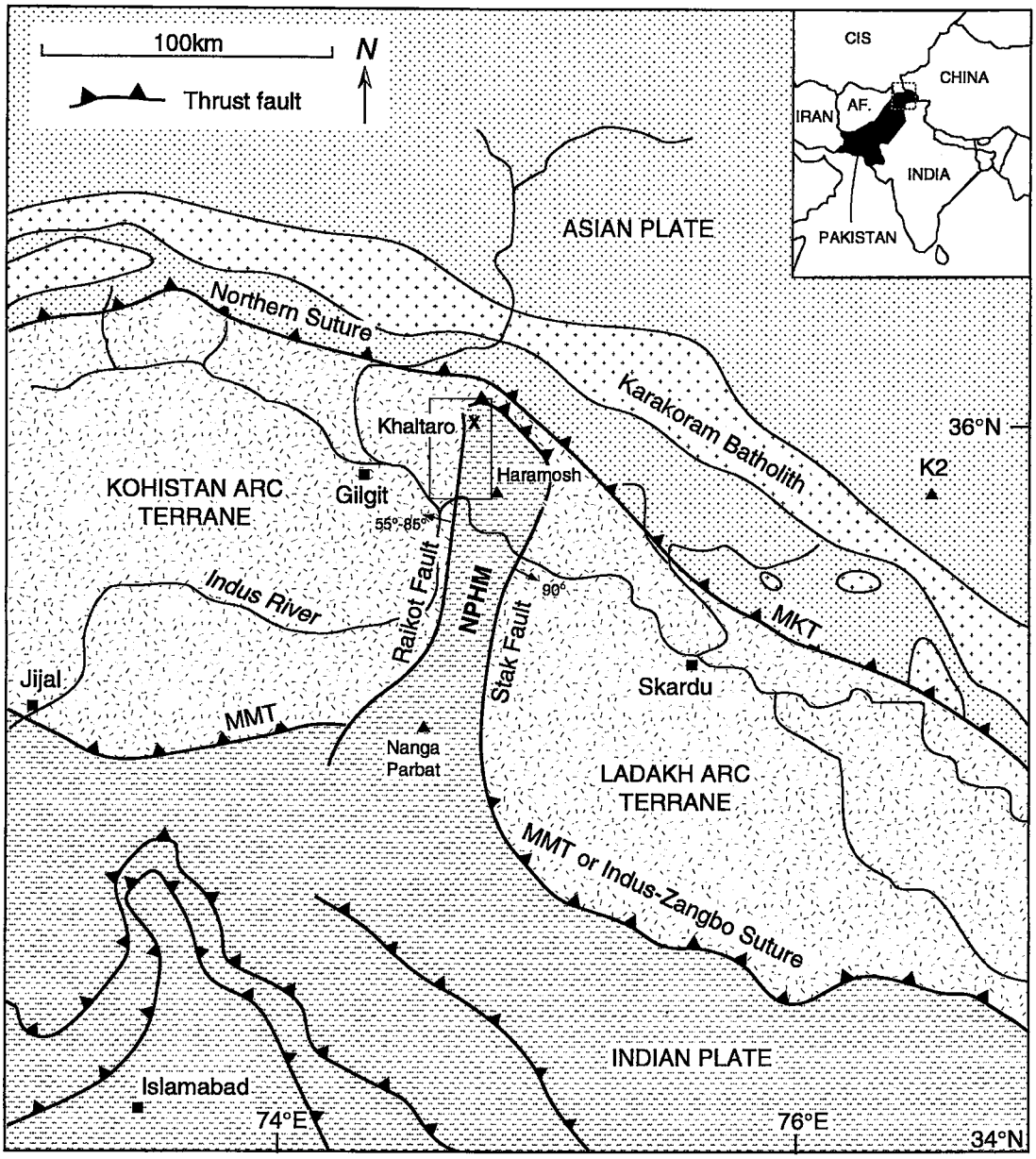

FIG. 1. Regional geological map of northern Pakistan [modified from Butler *et al.* (1992) and George *et al.* (1993)].

Zimbabwe, Kenya), South America (Brazil), Europe (Spain, Norway, Bulgaria), North America (North Carolina), and Australia (Kazmi & Snee 1989, Sinkankas 1989). These "schist-type" deposits [classified as exometamorphic by Sinkankas (1989)], are characterized by metasomatism of Cr-bearing ultramafic wallrocks into biotite or phlogopite schist adjacent to Be-bearing granitic pegmatites or hydrothermal veins. Emerald forms within the wall-rock schist (and rarely within the pegmatites or hydrothermal veins), where it may be accompanied by phenakite and chrysoberyl (Beus 1962, Martin-Izard *et al.* 1995). In spite of their prominence, few of these "schist-type" deposits have received detailed

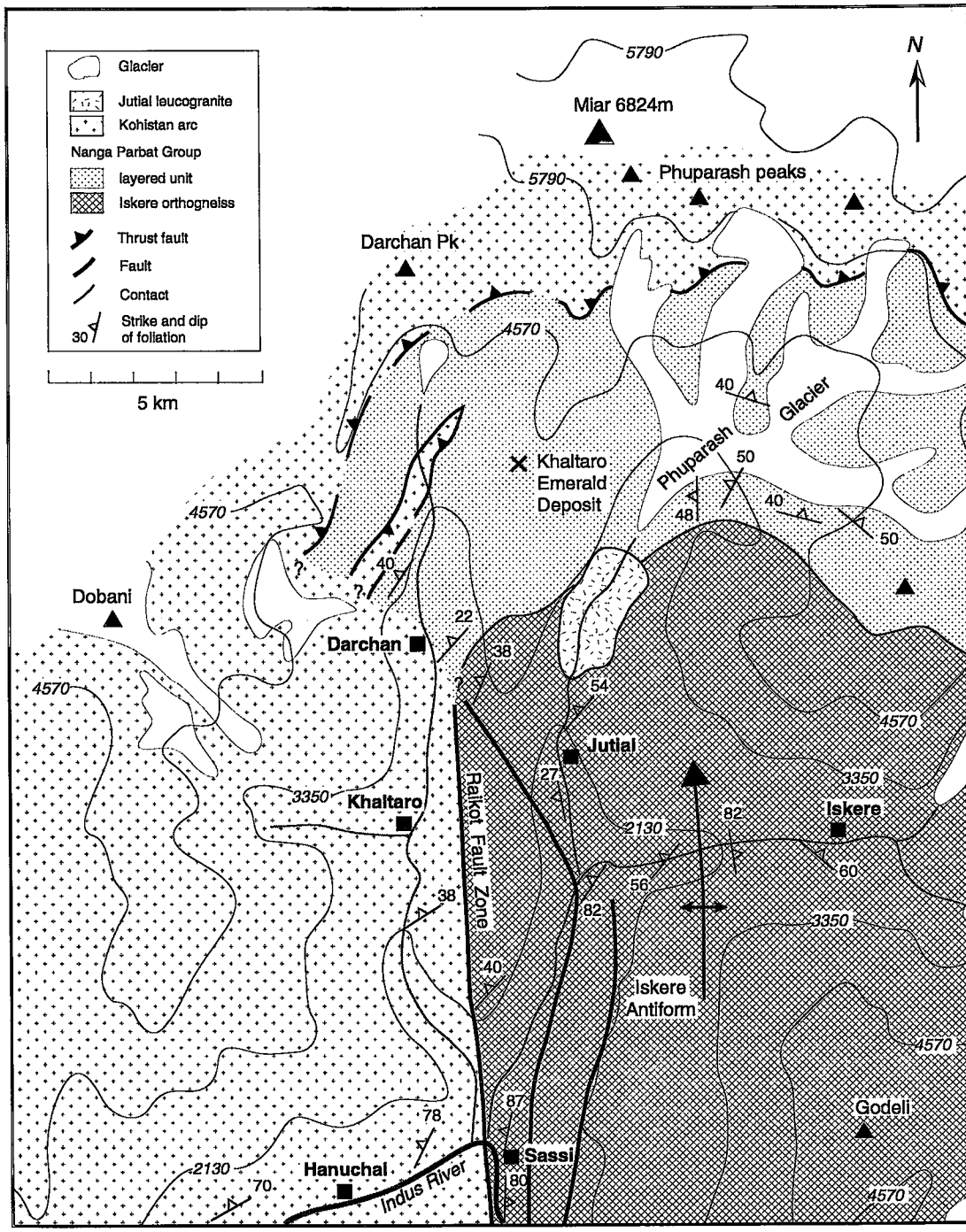

FIG. 2. Geology and structure of the Khaltaro area [modified from Madin (1986) and Butler *et al.* (1992)].

geochemical study (*e.g.*, Garstone 1981, Sliwa & Nguluwè 1984, Martin-Izard *et al.* 1995). Grundmann & Morteani (1989) examined the schist-hosted emerald deposits at Habachtal, Austria and Leydsdorp, South Africa, and proposed that emerald-bearing metasomatic zones at both locations are due to tectonic

juxtaposition of Cr- and Be-bearing rocks that was proceeded or accompanied by low-grade regional metamorphism. However at Khaltaro, field relations, petrography, and geochemistry indicate that emerald mineralization is a direct consequence of contact metasomatism of the amphibolite by the pegmatites and hydrothermal veins. The Khaltaro deposit is noteworthy because emerald forms inside, and not adjacent to, the pegmatite – hydrothermal vein system. This occurrence affords an excellent opportunity to study how metals and other chemical components are exchanged by hydrothermal fluids between the altered wallrock and the adjacent crystallizing pegmatite or vein. Characterization of the wallrock metasomatism allows quantification of wallrock sinks of chemical components derived from the pegmatite–vein magmatic–hydrothermal system, as well as wallrock sources that may have provided chemical components, in particular Cr and Fe, necessary to produce emerald mineralization.

Sampling and Analytical Procedures

Detailed geological mapping (scale 1:240) and sampling were done over a 13-day period in August, 1993. Outcrops and geology within the emerald-mineralized area (5000 m^2) were mapped from temporary benchmarks. Pegmatite and vein types were differentiated by their textures and dominant mineralogy. Detailed sketches (scale 1:12) of four outcrops (three containing emerald) recorded the mineralogy and texture of the pegmatites, veins, and adjacent altered wallrock. Precisely located samples (24) were collected from the sketched areas; several other samples were gathered from mine dumps and talus. Where possible, sequences of altered amphibolite were collected up to 20 cm from a given pegmatite or hydrothermal vein, along with samples of unaltered amphibolite that were located several meters away from any exposed veins.

The $^{40}Ar/^{39}Ar$ data were obtained by step-heating mineral separates at the U.S. Geological Survey, Denver, Colorado, using methods outlined in Snee *et al.* (1988). Concentrations of major and trace elements in whole-rock samples were established by X-ray fluorescence at the Geological Survey of Pakistan laboratory in Islamabad, and by instrumental neutron-activation analysis at Oregon State University (OSU). Chemical compositions of minerals were determined by electron microprobe at OSU. Plagioclase compositions reported herein were determined by electron-microprobe analysis unless stated otherwise. Analytical data are presented in Laurs (1995) (except for the $^{40}Ar/^{39}Ar$ data) and are available from the Depository of Unpublished Data, CISTI, National Research Council of Canada, Ottawa, Ontario K1A 0S2.

General Geology

The Khaltaro emerald deposit is located 70 km east-northeast of Gilgit, in the northwestern Haramosh massif near its contact with the Kohistan–Ladakh arc (Fig. 1). The Haramosh massif forms a northern extension of Indian plate basement, which has been rapidly exhumed from the tectonically overlying arc rocks over the past 10 Ma. The northern contact between the Haramosh massif and Kohistan–Ladakh terrane is a ductile shear that is interpreted to be the equivalent of the early-Tertiary-age Main Mantle Thrust (MMT) (Figs. 1, 2; Madin 1986, Madin *et al.* 1989, Butler & Prior 1988), which transported the arc rocks southward over the Indian plate during continental collision (Coward *et al.* 1988, Treloar *et al.* 1991). Late Cenozoic uplift of the Haramosh massif has occurred principally along northerly striking, steeply dipping mylonite shear-zones and younger brittle faults that reactivated the shears. These structures bound the Haramosh massif against the Kohistan–Ladakh arc: on the east is the Stak fault zone (Verplanck 1986), and on the west lies the Raikot (or Shahbatot) fault zone (Lawrence & Ghauri 1983, Madin 1986, Treloar *et al.* 1991). In the Khaltaro area, our reconnaissance field studies suggest that the Raikot fault truncates the older MMT, an observation consistent with Madin's (1986) conclusion that the Raikot fault is an active dextral reverse fault. Extremely rapid uplift (~6 mm/yr) of the Haramosh massif along the Raikot fault zone has occurred since late Quaternary time (Zeitler 1985, Zeitler *et al.* 1993), and has produced the maximum relief seen anywhere in the world (~7 km over a 25 km distance) along the western side of Nanga Parbat. Continued seismic activity is demonstrated by frequent earthquakes and numerous scarps cutting Holocene glacial till and alluvium in the Raikot fault zone (Madin 1986).

The Haramosh massif consists of Proterozoic orthogneiss and paragneiss with local biotite schist, calcschist, amphibolite, and marble (Madin 1986, Madin *et al.* 1989, Treloar *et al.* 1991). These rocks were called the Nanga Parbat Group and were broadly subdivided into the Iskere orthogneiss and the Shengus paragneiss by Madin (1986). Zeitler *et al.* (1989) obtained U–Pb zircon ages of 1850 Ma for the Iskere gneiss and 400 to 500 Ma for the Shengus gneiss. The gneissic sequence is folded along gently north-plunging fold axes to form the general domal structure of the north end of the Haramosh massif (Butler *et al.* 1992) (Fig. 2). The Khaltaro emerald deposit is apparently hosted by the "layered unit" of Butler *et al.* (1992), which consists of intercalated paragneiss and orthogneiss of intermediate composition, with thick layers of amphibolite, marble, and deformed sills of granitic rocks, that on the south structurally overlies the Iskere orthogneiss of Madin (1986) (Fig. 2).

The emerald deposit is hosted locally by complexly

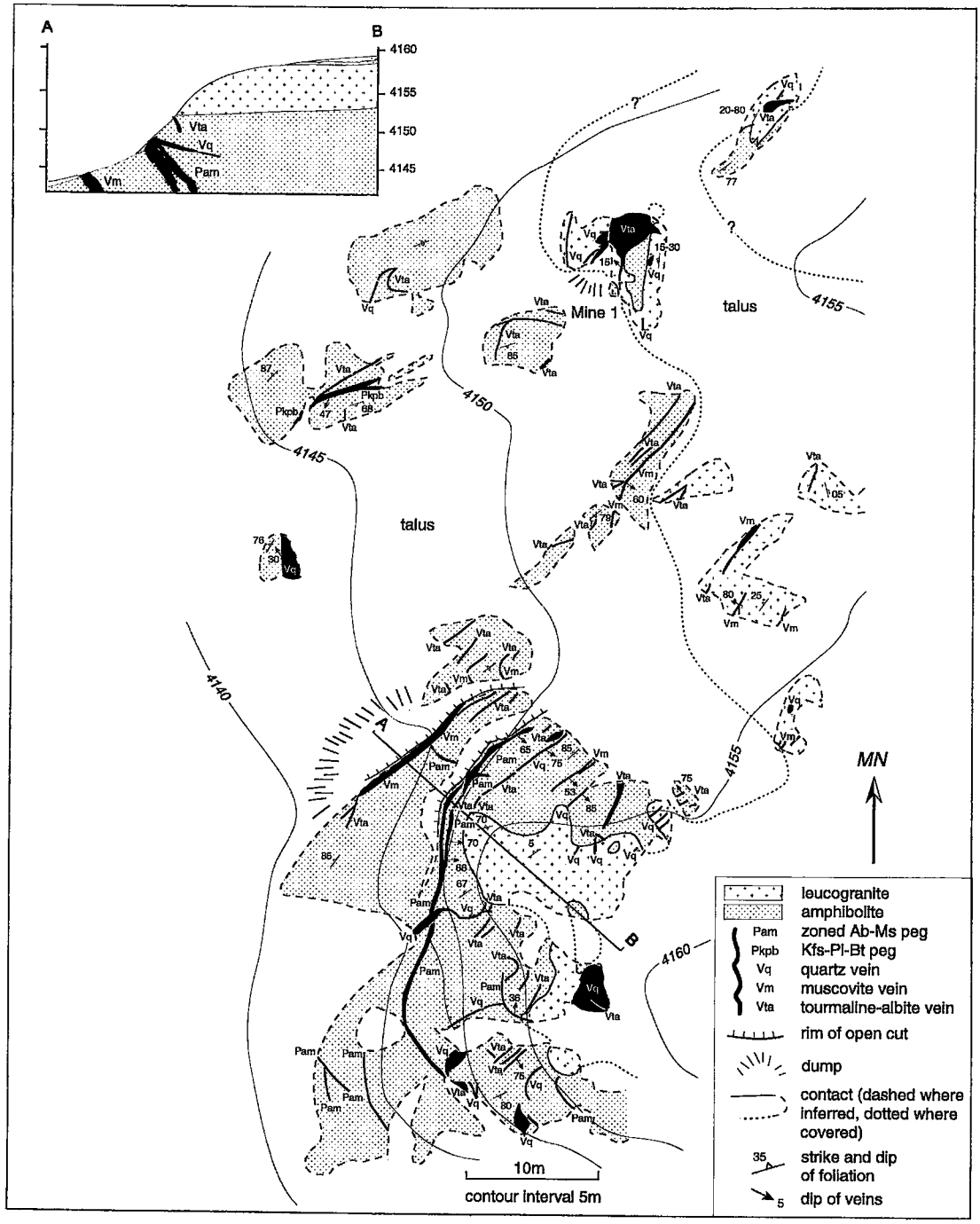

FIG. 3. Map and cross section of Khaltaro Mine 1 area.

folded garnet–mica schist and augen gneiss that conformably hosts a sill-like body of amphibolite. The foliation and compositional layering of these units dip moderately to steeply northwest, similar to the attitudes in the "layered unit" documented within 5 km of Khaltaro (Fig. 2). The amphibolite is at

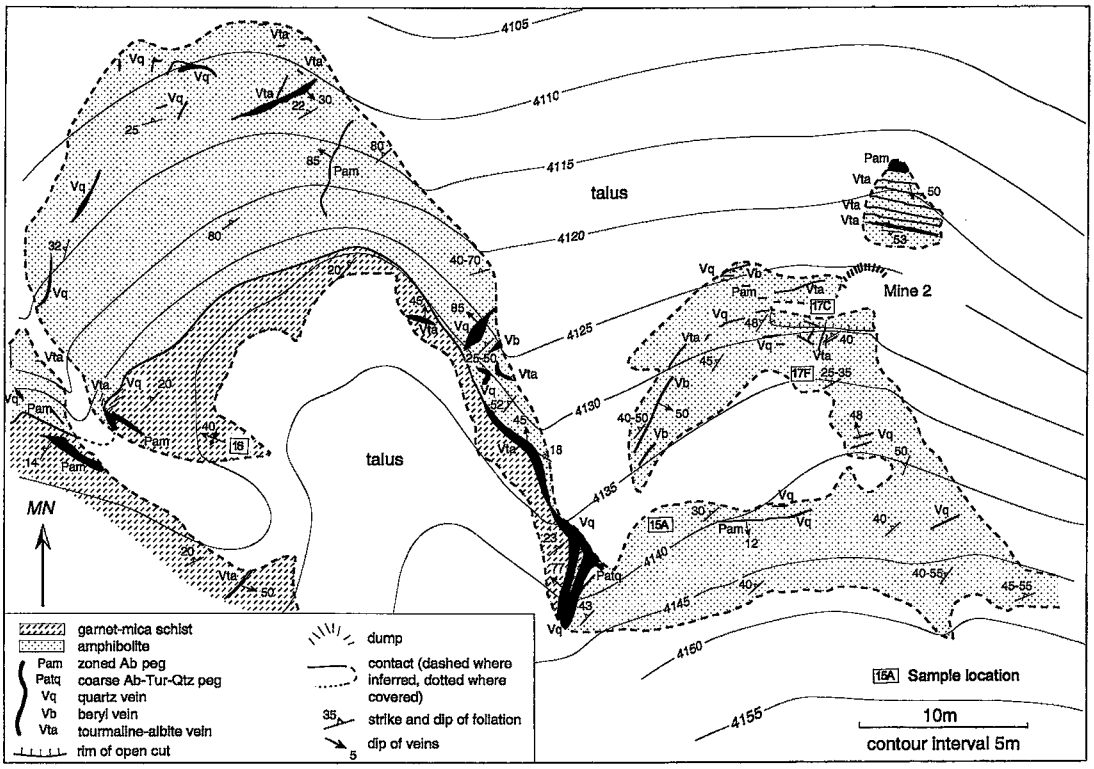

FIG. 4. Map of Khaltaro Mine 2 area.

least 40 m thick and exposed over an area of 5000 m^2, although talus obscures most contacts. Emerald mineralization is restricted to the margins of hydrothermal veins and albite-rich pegmatites that cross-cut and metasomatically alter the amphibolite. Two emerald prospects located 300 m apart within the amphibolite body will be referred to as Mine 1 and Mine 2, as per Kazmi *et al.* (1989). In the Mine 1 area, a leucogranite sill ranging from <1 m to at least 3 m thick discordantly intrudes the amphibolite, and is closely associated with several bodies of beryl-bearing granitic pegmatite and veins that locally host emerald (Fig. 3). At Mine 2, sparse pegmatites and veins cut amphibolite and garnet–mica schist (Fig. 4). According to local miners, Mine 2 yielded the largest production of emerald from quartz-rich hydrothermal veins cutting amphibolite (Fig. 4).

METAMORPHISM OF THE HARAMOSH MASSIF AND LEUCOGRANITE GENERATION

Peak metamorphism throughout most of the Nanga Parbat – Haramosh massif resulted in a granulite-facies migmatite complex (7–13 kbar and 600–800°C: Pognante *et al.* 1993, Treloar *et al.* 1994, Winslow *et al.* 1995). Treloar *et al.* (1994) suggested that this migmatite complex formed during Proterozoic peak metamorphism, and was subsequently re-metamorphosed to the amphibolite facies during Tertiary underthrusting of the Indian Plate along the MMT. In the Tato region of Nanga Parbat, subsequent Neogene high-temperature (>500°C) metamorphism, decompression-induced melting, and leucogranite emplacement occurred during rapid denudation of the massif (Smith *et al.* 1992, Zeitler *et al.* 1993, Winslow *et al.* 1995). Treloar *et al.* (1994) and Winslow *et al.* (1995) suggested that the Neogene metamorphism in the Nanga Parbat area was aided by heat that accompanied leucogranite emplacement.

In the northern portion of the Haramosh massif near Khaltaro, George *et al.* (1993) indicated that the "layered unit" cooled to <500–550°C by ~24 to 28 Ma on the basis of a Rb/Sr age on muscovite. However, the data we present below indicate that the "layered unit" at Khaltaro was not subjected to the high metamorphic grades observed elsewhere in the massif. The rocks reached a maximum metamorphic grade in the amphibolite facies during late Paleozoic time or before.

Postdating the peak of Tertiary metamorphism,

uplift of the Haramosh massif along bounding shears and faults was associated with the widespread emplacement of small leucogranite dikes, sills, and plutons. The bodies of leucogranite typically form coarse-grained, heterogeneous dikes 1 to 3 m wide and 10 to 100 m long (George *et al.* 1993). The dikes have sharp margins that cross-cut the metamorphic fabric, and are locally deformed near cataclastic and ductile shears (George *et al.* 1993). The leucogranites of the Nanga Parbat – Haramosh massif have been ascribed to fluid-absent decompression melting of a pelitic source undergoing rapid exhumation (Zeitler & Chamberlain 1991, George *et al.* 1993, Harris *et al.* 1993, Zeitler *et al.* 1993, Treloar *et al.* 1994). A fertile source for the Himalayan leucogranites could be shelf sediments of the Indian plate that were underthrust beneath the Kohistan–Ladakh arc and underwent Neogene to Recent metamorphism and melting due to rapid uplift (Treloar *et al.* 1994). U–Pb zircon ages of the leucogranites and pegmatite bodies in the Nanga Parbat – Haramosh massif are 5 to 8.2 Ma at Shengus, 30 km south of Khaltaro (Zeitler & Chamberlain 1991), and ~1 to 2.2 Ma at Tato, ~50 km south of Khaltaro (Zeitler *et al.* 1993).

Argon Geochronology

For three mineral samples from Khaltaro, we have obtained $^{40}Ar/^{39}Ar$ age spectra (Fig. 5). Amphibole from amphibolite and muscovite from mica schist were separated to evaluate the thermal history of the host rocks well removed from the pegmatites; muscovite was separated from the pegmatite. The low-potassium amphibole (0.15 to 0.34 wt% K_2O) yielded a disturbed spectrum, with a total gas age of 523 ± 2 Ma and an isochron age of 328 ± 40 Ma (Table 1, Fig 5a). Individual heating steps, excluding older ages related to excess Ar that are contained in the first eight steps (7.7% of ^{39}Ar released), range from 224.9 ± 1.5 Ma to 394.7 ± 0.7 Ma. These data suggest that the Tertiary Himalayan metamorphic event only partially degassed Ar from the amphibole, and therefore that it did not exceed ~550°C (blocking temperature: Snee *et al.* 1995). The metamorphic event that formed the amphibole likely occurred at 400 Ma or earlier, but later Paleozoic ages cannot be precluded because of the possibility of excess Ar. In contrast, the muscovite from the garnet–mica schist yields a disturbed spectrum that has been almost completely reset during the Himalayan metamorphism, which exceeded the 325°C blocking temperature of muscovite. This muscovite gave a $^{40}Ar/^{39}Ar$ total gas age of 10.03 ± 0.07 Ma and an isochron age of 8.56 ± 0.22 Ma, with heating steps ranging in age from 8.72 ± 0.06 to 13.69 ± 0.27 Ma (Table 1, Fig. 5b). The muscovite from a beryl-bearing pegmatite yielded a slightly disturbed $^{40}Ar/^{39}Ar$ spectrum, with a plateau age of 9.13 ± 0.04 Ma for three steps constituting 63.5% of the ^{39}Ar gas released

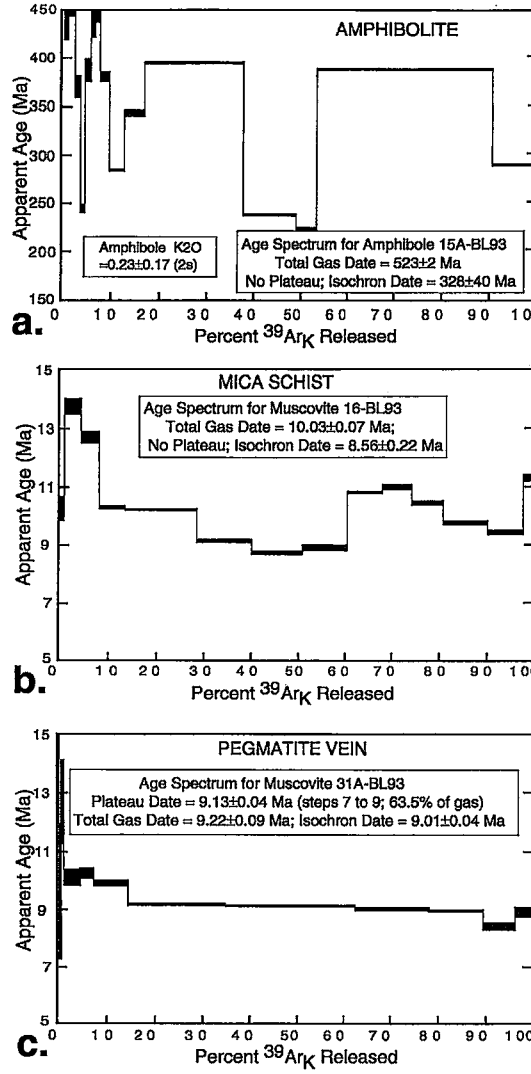

FIG. 5. $^{40}Ar/^{39}Ar$ age spectra for (a) calcic amphibole from amphibolite, (b) muscovite from garnet–mica schist, and (c) muscovite from an albitized beryl-bearing pegmatite vein ~30 m southeast of the Mine 1 area. See Figure 4 for location of samples of amphibolite and garnet–mica schist.

(Table 1, Fig. 5c).

The $^{40}Ar/^{39}Ar$ chronology indicates that the Proterozoic(?) rocks of the Khaltaro area were metamorphosed to the amphibolite facies in the Paleozoic or Proterozoic, but that Tertiary Himalayan metamorphic events were lower grade, with peak temperatures between 325 and 550°C. These data are consistent with Himalayan metamorphic temperatures at the lower end

TABLE 1. $^{40}Ar/^{39}Ar$ DATA FOR MINERAL SEPARATES[1] FROM SAMPLES OF GRANITIC PEGMATITE AND HOST ROCK, KHALTARO

Temp (°C)	Radiogenic ^{40}Ar [2]	K-derived ^{39}Ar [2]	$^{40}Ar_R/^{39}Ar_K$ [3]	$^{39}Ar/^{37}Ar$ [4]	Radiogenic yield (%)	Percent ^{39}Ar	Apparent age and error [5] (Ma)
15A-BL93; AMPHIBOLE; HOST-ROCK AMPHIBOLITE							
Total-gas date: 523 ± 2 Ma; no plateau; isochron date: 328 ± 40 Ma (850-1250°C); $(^{40}Ar/^{36}Ar)_i$ = 303 ± 32							
J = 0.006321, ±0.1%; wt., 287.6 mg							
600	5.203	0.0018	2881.0	0.03	93.9	0.5	5332.0 ± 1.8
700	1.039	0.0026	404.0	0.12	71.8	0.8	2286. ± 32.
800	0.4321	0.0047	92.2	0.19	69.4	1.4	828. ± 5.
850	0.1293	0.0036	36.0	0.08	45.1	1.1	370. ± 11.
900	0.0653	0.0028	23.0	0.07	38.4	0.9	245. ± 4.
950	0.1523	0.0040	37.8	0.06	61.7	1.2	387. ± 12.
975	0.1432	0.0032	44.6	0.03	53.8	1.0	448.9 ± 26.
1000	0.1941	0.0032	61.1	0.02	69.3	1.0	589. ± 12.
1025	0.2343	0.0063	37.1	0.02	62.6	1.9	380. ± 5.
1050	0.2679	0.0099	27.1	0.02	64.5	3.0	284.8 ± 1.4
1075	0.4636	0.0140	33.23	0.03	74.7	4.2	344. ± 3.
1100	2.6888	0.0695	38.70	0.03	90.2	20.8	394.7 ± 0.7
1125	0.8226	0.0366	22.46	0.03	73.8	11.0	239.5 ± 1.0
1175	0.3160	0.0150	21.00	0.03	53.0	4.5	224.9 ± 1.5
1250	4.7007	0.1240	37.90	0.03	91.3	37.2	387.4 ± 0.5
1400	0.8849	0.0321	27.56	0.03	75.0	9.6	289.7 ± 0.8
16-BL93; MUSCOVITE; HOST-ROCK MICA SCHIST							
Total-gas date: 10.03 ± 0.07 Ma; no plateau; isochron date: 8.56 ± 0.22 Ma (600-1300°C); $(^{40}Ar/^{36}Ar)_i$ = 381 ± 11							
J = 0.006235, ±0.1%; wt., 87.2 mg							
500	0.0666	0.0733	0.909	--	25.2	1.2	10.2 ± 0.4
600	0.2491	0.2038	1.222	--	40.7	3.4	13.69 ± 0.27
650	0.2465	0.2185	1.128	--	63.1	3.7	12.64 ± 0.20
700	0.2861	0.3135	0.912	--	52.8	5.3	10.23 ± 0.05
750	0.8043	0.8880	0.906	--	65.8	14.9	10.16 ± 0.02
800	0.5559	0.6842	0.812	--	76.9	11.5	9.11 ± 0.06
850	0.5004	0.6436	0.778	--	74.5	10.8	8.72 ± 0.06
900	0.4536	0.5726	0.792	--	67.7	9.6	8.89 ± 0.09
950	0.4283	0.4455	0.961	--	70.0	7.5	10.78 ± 0.03
1000	0.3532	0.3608	0.979	--	65.5	6.1	10.98 ± 0.10
1050	0.3658	0.3940	0.929	--	66.6	6.6	10.41 ± 0.08
1100	0.4952	0.5693	0.870	--	69.4	9.6	9.76 ± 0.06
1150	0.3578	0.4253	0.841	--	69.2	7.1	9.44 ± 0.06
1300	0.1602	0.1587	1.009	--	50.0	2.7	11.32 ± 0.10

TABLE 1 (continued)

Temp (°C)	Radiogenic ^{40}Ar [2]	K-derived ^{39}Ar [2]	$^{40}Ar_R/^{39}Ar_K$ [3]	$^{39}Ar/^{37}Ar$ [4]	Radiogenic yield (%)	Percent ^{39}Ar	Apparent age and error [5] (Ma)
31A-BL93; MUSCOVITE; GRANITIC PEGMATITE							
Total-gas date: 9.22 ± 0.09 Ma; plateau date: 9.13 ± 0.04 Ma; isochron date: 9.01 ± 0.04 Ma (800-1050°C); $(^{40}Ar/^{36}Ar)_i$ = 322 ± 22							
J = 0.006112, ±0.1%; 53 mg							
500	0.0239	0.0175	1.36	--	14.0	0.4	15.0 ± 2.7
600	0.0167	0.0191	0.87	--	14.3	0.4	9.6 ± 2.3
650	0.0308	0.0267	1.15	--	25.5	0.6	12.7 ± 1.4
750	0.1290	0.1402	0.920	--	26.8	3.2	10.11 ± 0.28
800	0.1116	0.1197	0.932	--	37.2	2.7	10.25 ± 0.17
850	0.2818	0.3123	0.902	--	56.5	7.2	9.92 ± 0.08
900[P]	0.7493	0.8978	0.835	--	82.9	20.6	9.18 ± 0.05
950[P]	0.9924	1.1950	0.830	--	85.2	27.4	9.13 ± 0.02
1000[P]	0.5574	0.6784	0.822	--	89.8	15.5	9.04 ± 0.06
1050	0.4057	0.4973	0.816	--	90.2	11.4	8.97 ± 0.05
1100	0.2261	0.2942	0.769	--	88.1	6.7	8.46 ± 0.13
1300	0.1358	0.1669	0.814	--	87.0	3.8	8.95 ± 0.17

[1] Samples were crushed, ground, and sieved, and the 80 to 120 mesh-size sieve fractions were passed through a magnetic separator. The concentrates were hand picked to 100% purity, and cleaned in reagent-grade ethanol, acetone, and de-ionized water in an ultrasonic bath. The samples were wrapped in aluminum packages and sealed in silica vials along with monitor minerals prior to irradiation in the TRIGA reactor at the U.S. Geological Survey in Denver, Colorado for 28.75 hours at 1 megawatt.

[2] A Mass Analyzer Products 215 Rare Gas mass spectrometer with a Faraday cup was used to measure argon-isotope abundances. Abundances of "Radiogenic ^{40}Ar" and "K-derived ^{39}Ar" are reported in volts. Conversion to moles can be made using 9.74×10^{-13} moles argon per volt of signal. Detection limit at the time of this experiment was 2×10^{-17} moles argon. Analytical data for "Radiogenic ^{40}Ar" and "K-derived ^{39}Ar" are calculated to five decimal places; "$^{40}Ar_R/^{39}Ar_K$" is calculated to three decimal places. "Radiogenic ^{40}Ar", "K-derived ^{39}Ar", and "$^{40}Ar_R/^{39}Ar_K$" are rounded to significant figures using analytical precisions. Apparent ages and associated errors were calculated from unrounded analytical data and then each rounded using associated errors. All analyses were done in the Argon Laboratory, U.S. Geological Survey, Denver, Colorado. Decay constants used are those of Steiger & Jäger (1977), *i.e.*, $\lambda_e = 0.581 \times 10^{-10}$/yr., $\lambda_\beta = 4.962 \times 10^{-10}$/yr., $\lambda = \lambda_e + \lambda_\beta = 5.543 \times 10^{-10}$/yr. The irradiation monitor, hornblende MMhb-1 with percent K = 1.555, $^{40}Ar_R = 1.624 \times 10^{-9}$ mole/g, and K-Ar age = 520.4 Ma (Samson & Alexander 1987), was used to calculate J values for this experiment.

[3] "$^{40}Ar_R/^{39}Ar_K$" has been corrected for all interfering isotopes, including atmospheric argon. Mass discrimination in our mass spectrometer was determined by measuring the $^{40}Ar/^{36}Ar$ ratio of atmospheric argon. Our measured value is 298.9 during the period of this experiment; the accepted atmospheric $^{40}Ar/^{36}Ar$ ratio is 295.5. Abundances of interfering isotopes of argon from K and Ca were calculated from reactor production-ratios determined by irradiating and analyzing pure CaF_2 and K_2SO_4 simultaneously with these samples. The measured production-ratios for these samples are $(^{40}Ar/^{39}Ar)_K = 7.92 \times 10^{-3}$, $(^{38}Ar/^{39}Ar)_K = 1.309 \times 10^{-2}$, $(^{37}Ar/^{39}Ar)_K = 1.75 \times 10^{-4}$, $(^{36}Ar/^{37}Ar)_{Ca} = 2.68 \times 10^{-4}$, $(^{39}Ar/^{37}Ar)_{Ca} = 6.85 \times 10^{-4}$, and $(^{38}Ar/^{37}Ar)_{Ca} = 4.40 \times 10^{-5}$. Corrections also were made for additional interfering isotopes of argon produced from irradiation of chlorine using the method of Roddick (1983). The reproducibility of split gas-fractions from each monitor (0.05-0.25%, 1 σ) was used to calculate imprecisions in J. J values for each sample were interpolated from adjacent monitors and have similar uncertainties to the monitors. Uncertainties in calculations for the date of individual steps in a spectrum were calculated using modified equations of Dalrymple *et al.* (1981).

[4] To calculate apparent K/Ca ratios, divide the $^{39}Ar/^{37}Ar$ ratio value by 2; -- indicates that ^{37}Ar was not present during analysis above background level.

[5] 1 σ error.

[P] Fraction included in plateau date.

of the range <500 to 550°C (at 28 to 24 Ma) inferred by George *et al.* (1993). The muscovite in both the pegmatite and garnet–mica schist record the same age of 9 Ma, which represents cooling through the ~325°C isotherm. The pegmatites, which have solidus temperatures of ~600°C, must therefore have been emplaced into wallrocks that were much cooler. The pegmatites could be significantly older than 9 Ma, and are clearly older than the 5 to 8.2 Ma crystallization ages of the pegmatites at Shengus (Zeitler & Chamberlain 1991), and the ~1 to 2.2 Ma ages of crystallization of leucogranite and pegmatite bodies located farther south in the Tato region (Zeitler *et al.* 1993). These data support the diachronous nature of Neogene leucogranite and pegmatite magmatism within the Nanga Parbat – Haramosh massif, with ages decreasing to the south.

Petrology and Geochemistry

Rocks found within the immediate study area consist of garnet–mica schist, amphibolite, leucogranite, granitic pegmatites (four types), and hydrothermal veins (four types).

Garnet–mica schist

Subdued, rusty-gray outcrops of garnet–mica schist are locally intruded by concordant lenses and irregular cross-cutting veins of pegmatite and quartz. These veins locally contain beryl, but not emerald. The schist is light gray on its fresh surface and consists of fine-grained, thinly laminated biotite and muscovite with intercalated quartz- and plagioclase-dominant layers up to 1 cm wide. The typical mode is quartz (40–50%), biotite (20–25%), muscovite (15–20%), plagioclase (3–5%, reversely zoned, An_{10-25}), and traces of Fe–Ti oxides and zircon. Porphyroblasts of deep purple garnet (1–5%; unzoned, $Alm_{73}Prp_{17}Grs_7Sps_3$) are disseminated. In places, the garnet is partially or completely replaced by muscovite ± biotite aggregates. These textures are consistent with biotite and garnet compositions that indicate lack of chemical equilibrium (Ferry & Spear 1978). The mineral assemblage suggests conditions of peak metamorphism of 550 to 600°C at medium pressures. The mineralogy, laminated texture and chemical composition (Table 2) of the garnet–mica schist suggest a shale protolith. In trace-element profile, the schist is nearly identical to the North American Shale Composite (Fig. 6).

Amphibolite

The amphibolite forms rounded, gray-green, resistant outcrops that are conspicuously banded compositionally on a cm- to m-scale, moderately foliated, and cross-cut by pegmatite dikes and veins. Two varieties of amphibolite are defined, plagioclase amphibolite and zoisite amphibolite, on the basis of relative modal abundances (Table 3). The two types of amphibolite are difficult to distinguish in the field and locally grade into one another. They are broadly intercalated on a m-scale in the Mine 2 area, whereas the Mine 1 area is dominated by zoisite amphibolite. Emerald-bearing hydrothermal veins and pegmatite bodies are hosted by both types of amphibolite.

The plagioclase amphibolite consists of moderately foliated, medium-grained (1–3 mm) calcic amphibole [unzoned, pargasite to tschermakite, according to Leake (1978)], plagioclase (An_{20-60}), local garnet (unzoned, $Alm_{56}Prp_{18}Grs_{18}And_2Sps_6$), and accessory titanite, rutile, apatite, pyrite, ilmenite, and zircon (Table 3). The zoisite amphibolite consists of weakly foliated, coarse-grained (3–5 mm) calcic amphibole (unzoned magnesiohornblende), zoisite, plagioclase (An_{40-80}), and sporadic garnet (unzoned, $Prp_{40}Alm_{38}Grs_{20}Sps_2$), with accessory calcite, zircon, rutile, and titanite (Table 3). These assemblages are consistent with formation at the amphibolite or upper epidote–amphibolite facies. The garnet contains tiny inclusions (<0.01 mm) of oriented rutile (?) needles, and is locally rimmed by fine-grained (0.5–1 mm), zoned, strongly pleochroic amphibole (edenite–pargasite) with quartz and local rutile. The Cr content of the garnet is generally below detection limit of the electron microprobe (0.07 wt% Cr_2O_3). The

TABLE 2. GEOCHEMISTRY OF MICA SCHIST AND AMPHIBOLITE, KHALTARO

	mica schist	plagioclase[1] amphibolite (n=3)		zoisite[1] amphibolite (n=4)	
SiO_2 (wt.%)	70.67	51.48	(0.61)	45.61	(1.01)
TiO_2	0.74	0.67	(0.41)	0.30	(0.15)
Al_2O_3	14.14	14.93	(0.31)	19.05	(1.87)
$Fe_2O_3^T$	6.30	10.35	(1.24)	6.48	(1.13)
MnO	0.11	0.19	(0.04)	0.29	(0.33)
MgO	1.16	8.38	(2.16)	10.57	(2.02)
CaO	0.52	9.47	(0.97)	15.08	(1.50)
Na_2O	0.65	3.62	(1.02)	1.44	(0.17)
K_2O	3.87	0.24	(0.15)	0.37	(0.32)
P_2O_5	0.06	0.33	(0.53)	0.10	(0.16)
LOI	1.89	1.13	(0.47)	1.17	(0.35)
Σ wt.%	100.11	100.80	(0.73)	100.44	(0.11)
Sc (ppm)	15.5	40.5	(2.51)	32.1	(9.20)
V	102	342	(24)	286	(276)
Cr	181	399	(344)	331	(268)
Ni	30	106	(95)	166	(110)
Cu	14	53	(36)	16	(29)
Zn	95	97	(28)	39	(20)
Ga	19	14	(3)	15	(5)
As	1.7	<8.2		12.1	(6.0)
Sb	<0.23	<0.30		0.21	(0.01)
Se	1.1	<3.5		<3.7	
Rb	170	17	(18)	74	(61)
Cs	9.63	8.38	(11.73)	13.8	(9.57)
Sr	56	96	(27)	101	(78)
Ba	602	<28		<76	
La	38.1	1.7	(1.4)	1.7	(1.7)
Ce	77.3	<4.2		2.6	(1.0)
Nd	31.9	5.0	(2.0)	2.5	(0.8)
Sm	6.62	1.44	(1.06)	1.26	(1.21)
Eu	1.12	0.58	(0.40)	0.59	(0.43)
Tb	0.79	0.42	(0.26)	0.30	(0.24)
Yb	3.07	1.84	(0.73)	0.86	(0.42)
Lu	0.45	0.29	(0.15)	0.16	(0.11)
Y	26	19	(9)	10	(7)
Zr	238	23	(29)	3	(3)
Hf	7.24	1.04	(0.73)	0.39	(0.05)
Nb	14	1	(0)	<1	
Ta	0.90	<0.14		<0.17	
Hg	<0.16	<0.17		<0.19	
Tl	<10	<10		<10	
Th	15.0	<0.9		<2.0	
U	2.8	<3.4		<5.9	

Major elements by XRF with errors of ±1-2% using Rigaku 3370E on fused glass disks with 1:5 ratio rock to Li tetraborate; trace elements by XRF on pressed pellets (±5-10%) for V, Cr (>100 ppm), Ni, Cu, Zn, Ga, Rb, Sr, Ba, Y, Zr, Nb, & Tl. Other trace elements by INAA using the O.S.U. TRIGA reactor (flux = $3x10^{12}$ thermal neutrons/cm^2-sec), a 2048 channel PHA, and computer data reduction; errors are ±5%, except Sc & La (3%), Co (5-10%), Ce & U (7%), Nd (12%).
In parentheses, are one standard deviation of mean (n samples).
[1] Sample numbers are listed in Table 3.

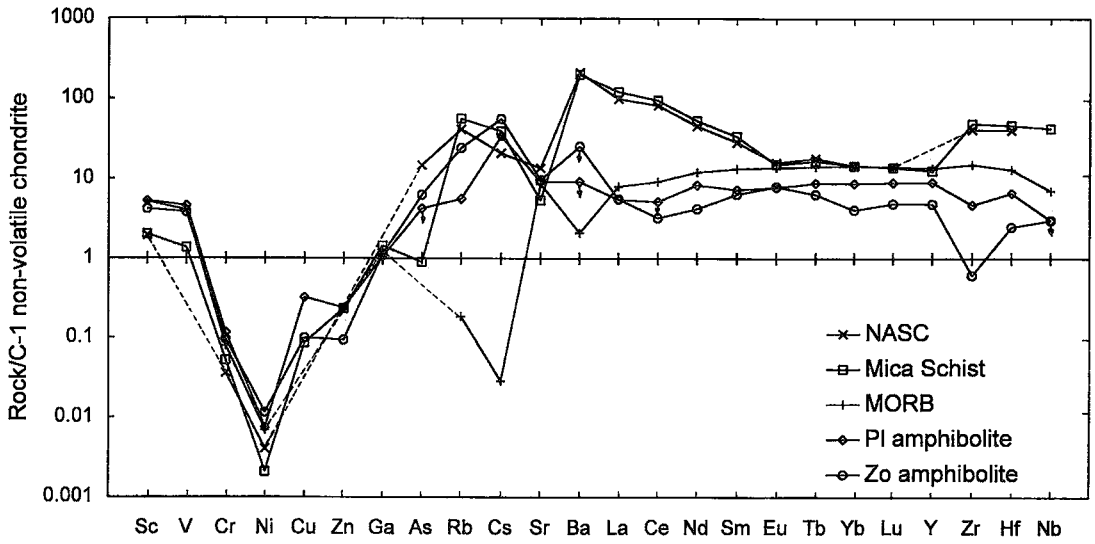

FIG. 6. Chondrite-normalized trace-element abundances of the host rocks at Khaltaro. Supplied for comparison are NASC, the North American Shale Composite of Gromet *et al.* (1984), and MORB, the average Mid-Ocean Ridge Basalt of Sun & McDonough (1989) and Pearce & Parkinson (1993); chondrite values from Anders & Ebihara (1982). Host-rock composition is averaged for plagioclase amphibolite (three samples) and zoisite amphibolite (four samples) (Table 1). Dashed lines are drawn through areas with missing data, and arrows indicate upper limits. Concentrations of Sb, Se, Hg, Tl, Ta, Th, and U are not shown owing to insufficient data.

amphiboles are characterized by widely variable molar Mg/(Mg + Fe) and Al/(Al + Si) values, with Cr contents ranging up to 0.60 wt% Cr_2O_3 (average 0.08 wt%). The zoisite is Fe-rich (up to 6.5 wt% $Fe_2O_3^T$) and contains significant Cr (up to 0.87, average 0.15 wt% Cr_2O_3). Amphibole and zoisite are the principal carriers of Cr in the amphibolite; no distinct Cr minerals were noted. Biotite in the "unaltered" amphibolite forms sparse optically continuous poikiloblasts, replacements of amphibole along cleavages, and cross-cutting veinlets with plagioclase ± quartz. This biotite contains 0.54 to 0.60 wt% F, and therefore probably has equilibrated with fluids released from local pegmatites or hydrothermal veins.

The plagioclase amphibolite and, to a greater extent, zoisite amphibolite, contain depleted contents of rare-earth elements (*REE*) and high-field-strength elements

TABLE 3. MODAL VARIATION IN UNALTERED AMPHIBOLITE, KHALTARO

	Plagioclase amphibolite			Zoisite amphibolite			
Sample	15A	15B	17F	17E	26G	28F	29
Area	Mine 2	Mine 2	Mine 2	Mine 2	Mine 1	Mine 1	Mine 1
Dist. to vein	5 m	5 m	3.6 m	1.5 m	0.9 m	8 m	? (talus)
VOLUME %							
Amphibole	60	63	80	83	80	85	80
Plagioclase	37	35	20	1	1	8	tr
Zoisite	0	0	tr	15	18	7	10
Garnet	3	2	tr	0	0	0	10
Biotite*	0	0	tr	1	1	0	0
Accessories	Ttn,Ap,Qtz, zircon,rutile	Ttn,Ap,Py, ilmenite	zircon	calcite	zircon	(none)	rutile

* Biotite is of probable metasomatic origin.
Note: Modal data estimated from thin sections. Mineral symbols are from Kretz (1983).

(*HFSE*) relative to mid-ocean-ridge basalt (Fig. 6). Compared to plagioclase amphibolite, the zoisite amphibolite contains more Al, Mg, and Ca, and less Si, Fe, and Na (Table 2). Both types of amphibolite have been enriched in Rb and Cs, presumably owing to hydrothermal fluids of pegmatitic origin. The amphibolite protolith was probably an internally differentiated tholeiitic or MORB-like gabbroic sill or thick basalt flow, as suggested by field relations, textural and compositional layering, and the geochemical data. The enrichment of Al, Mg, and Ca in the zoisite amphibolite is proposed to be the result of abundant cumulate plagioclase and pyroxene, whereas *HFSE* and *REE* depletion is due to concentration of these elements in silicate liquid excluded from the pile of cumulus minerals.

Leucogranite

A sill-like sheet of leucogranite intrudes amphibolite in the Mine 1 area, and crops out over an area of about 80 m × 15 m (Fig. 3). The leucogranite is heterogeneous and consists of porphyroclastic granite and subordinate biotite granite that is locally albitized. South of Mine 1, the granite body is at least 3 m thick, nearly flat-lying, and discordantly intrudes the amphibolite. To the north, the granite thins to 1 m and dips steeply northwest, concordant with foliation in the amphibolite. Weak foliation within the granite is parallel to the contacts, and is defined by layers of porphyroclastic feldspar and fine-grained biotite. Abundant bodies of pegmatite and hydrothermal veins cross-cut the granite and extend outward into the adjacent amphibolite. The granite, bodies of pegmatite, and veins are slightly deformed where the host amphibolite contains subtle folds and changes in orientation. Deformation has resulted in subparallel elongation of mineral grains and sutured boundaries of the quartz grains.

The granite seen in most exposures is gneissic, containing medium-grained porphyroclastic K-feldspar and plagioclase (1 to 2 cm; An_{20}), with intergranular quartz, plagioclase, and scarce biotite (2%). The proportion of quartz to K-feldspar to plagioclase is approximately 30:25:40, a true granite according to International Union of Geological Sciences nomenclature (Streckeisen 1976). Muscovite, chlorite (as inclusions in K-feldspar), pyrite, and rutile are accessory phases. Foliated aggregates of biotite intergrown with subordinate granular plagioclase and quartz form layers that are bent around feldspar porphyroclasts. Cross-hatched twinning of K-feldspar is seen rarely along grain rims.

The porphyroclastic granite shows some geochemical similarities to other examples of Himalayan leucogranite, such as the nearby Jutial two-mica leucogranite (Butler *et al.* 1992) (Table 4, Fig. 7). The Himalayan leucogranites are peraluminous, with high

TABLE 4. GEOCHEMISTRY OF KHALTARO AND JUTIAL LEUCOGRANITES

Location Descript.	Jutial*	Khaltaro porphyroblastic	Khaltaro biotite-rich	Khaltaro albitized
SiO_2 (wt%)	73.63	72.79	62.29	64.29
TiO_2	0.10	0.03	0.55	0.10
Al_2O_3	14.79	15.62	18.68	20.58
$Fe_2O_3^T$	1.00	0.52	3.89	0.39
MnO	0.01	0.01	0.04	0.03
MgO	0.14	0.14	1.29	0.27
CaO	1.20	1.84	1.49	1.57
Na_2O	3.54	4.22	3.98	9.05
K_2O	5.16	4.56	7.28	2.86
P_2O_5	0.05	0.00	0.05	0.00
LOI	n.d.	0.82	1.36	1.17
Σ wt.%	99.63	100.56	100.89	100.32
Trace elements				
Sc (ppm)	n.d.	1.30	5.54	2.96
V	n.d.	<7	40	9
Cr	n.d.	2.2	10.6	2.7
Ni	n.d.	5	11	4
Cu	n.d.	59	4	<1
Zn	n.d.	5	75	19
Ga	n.d.	18	21	34
As	n.d.	19.9	2.0	1.4
Sb	n.d.	0.11	<0.24	0.08
Se	n.d.	2.5	1.8	5.2
F	n.d.	160	700	n.d.
B	n.d.	25	15	n.d.
Be	n.d.	6.0	2.7	n.d.
Li	n.d.	58	215	n.d.
Rb	294	168	270	401
Cs	n.d.	11.4	44.4	27.0
Sr	83	450	743	410
Ba	221	1222	3094	1735
La	n.d.	3.5	7.3	1.8
Ce	55.4	13.6	15.0	3.8
Nd	n.d.	9.6	8.4	2.4
Sm	4.0	<0.14	1.21	0.51
Eu	n.d.	0.45	0.85	0.55
Tb	n.d.	0.14	0.10	0.11
Yb	0.9	0.83	0.60	0.84
Lu	n.d.	<0.10	0.12	0.11
Y	12	5	2	<1
Zr	47	65	131	46
Hf	1.7	2.26	3.46	1.09
Nb	11	10	14	12
Ta	1.3	1.57	0.64	2.95
Hg	n.d.	<0.05	<0.10	<0.07
Tl	n.d.	<10	<10	<10
Th	22	1.9	3.4	0.9
U	20	48.5	3.5	1.1

Note: Analyzed by Chemex Labs, Inc. are Li & Be by atomic absorption, and B by INAA, and F by specific ion electrode; detection limits for Li, Be, B, and F are 1, 0.1, 5, & 20 ppm, respectively.
* Average of 11 analyses from George et al. (1993): Ta, Hf, Ce, Sm, & Yb by INAA; all others by XRF.

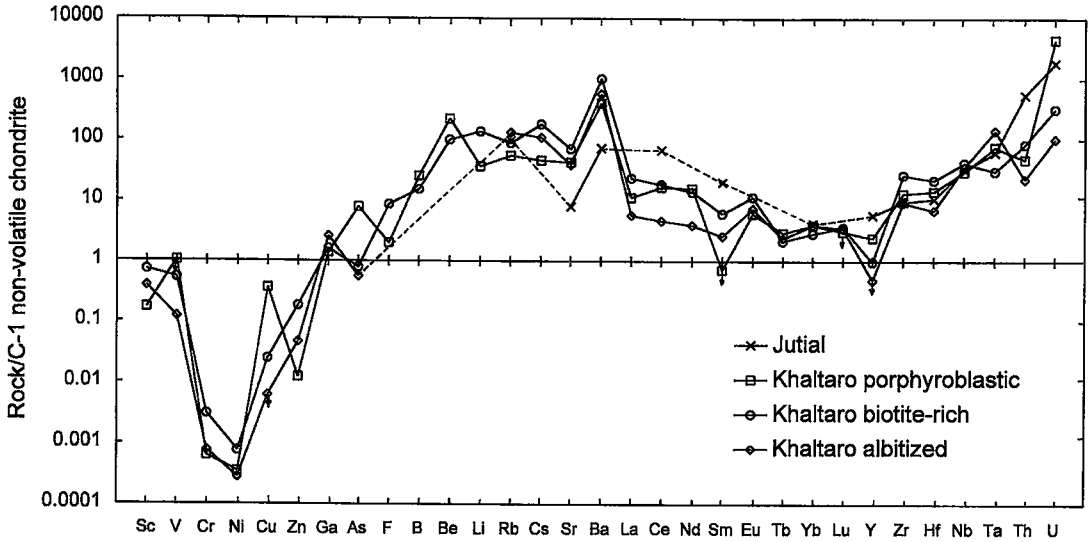

FIG. 7. Chondrite-normalized trace-element abundances of leucogranites at Khaltaro. The Jutial leucogranite is supplied for comparison (George *et al.* 1993). Chondrite values from Anders & Ebihara (1982). Dashed lines are drawn through areas with missing data, and arrows indicate upper limits. Concentrations of Sb, Se, Hg, Tl are not shown owing to insufficient data.

levels of silica (>70%), Rb/Sr (3 to 23), and alkalis (*cf.* K and Rb), and depleted in Ca and *HFSE* (*cf.* Y and Zr) (Harris *et al.* 1986, George *et al.* 1993). These characteristics are attributed to incongruent melting of a muscovite-rich metasedimentary source (Scaillet *et al.* 1990, Harris & Inger 1992). The leucogranitic rocks are generally depleted in Ba and Sr compared to potentially parental metasedimentary gneiss (George *et al.* 1993). However, the Khaltaro leucogranite is enriched in Ba and Sr (Fig. 7), and has Rb/Sr less than 1. Harris *et al.* (1993) attributed low Rb/Sr values to vapor-saturated, disequilibrium partial melting of a feldspathic source, such as greywacke.

In the central and southern outcrops, the Khaltaro leucogranite contains both porphyroclastic granite and layers of biotite-rich granite. This biotite-bearing granite is fine- to medium-grained and contains equigranular microcline (52%), plagioclase (30%), quartz (10%), and biotite (8%). A subtle foliation is suggested by subparallel orientation of fine-grained biotite. Muscovite, chlorite (after biotite), and apatite are accessories; pyrite is absent. K-feldspar commonly shows cross-hatched twinning, and plagioclase (An_{17} by optical determination) contains abundant myrmekite and is partly altered.

The *REE* patterns of the biotite-bearing granite and the porphyroclastic granite are similar (Table 4, Fig. 7), suggesting a genetic relationship. Despite this similarity, the biotite-bearing granite contains much higher levels of K, Al, Fe, Mg, Ti, Ba, Sr, Li, F, and Cs, slightly higher concentrations of Rb, and lesser Si (Table 4, Fig. 7). The geochemical differences may be attributed to greater mobility of elements in the relatively F-rich magma [*e.g.*, Grinberg (1951) in Solov'yev *et al.* (1967)] that gave rise to the biotite-bearing granite. Relatively higher amounts of Cr, V, and Fe suggest that the biotite-bearing granitic magma experienced greater interaction with the surrounding amphibolites than did the magma that gave rise to the porphyroclastic rock. However, amphibolite adjacent to the leucogranite shows no evidence of alteration, except in places where the leucogranite is albitized.

The biotite-bearing granite is locally altered into a distinct albitized granite dominated by albite ($An_{<3}$), with subordinate K-feldspar (<20%), quartz (<10%) and muscovite (9%). Traces of fluorite also are present, whereas mafic minerals and sulfides are absent. The albitization is sporadic, and in places surrounds hydrothermal segregations and cross-cutting veins containing assemblages of quartz, muscovite, albite, and tourmaline. Locally, quartz seems to have been leached from the albitized granite, leaving small (<1 cm) miaroles containing euhedral crystals of albite. Albitization caused the conversion of biotite to muscovite, and alteration of some K-feldspar into albite with the addition of local muscovite and fluorite. Chemical changes accompanied the albitization of the biotite granite: increase in Na, Al and Si, and decrease in Fe, Mg, K, and Ti (Table 4). Rb and Ta are also

enriched, whereas most other trace elements are depleted (Fig. 7). The presence of disseminated fluorite indicates enrichment in F. Fluoride complexing may have provided further mobility of the various major and trace elements, which were gained or lost during albitization.

Pegmatites

Pegmatite dikes are common in proximity to the leucogranite in the Mine 1 area, where they are thin (<1.5 m wide), continuous, and simply zoned. In the Mine 2 area, however, pegmatite forms rare lenticular

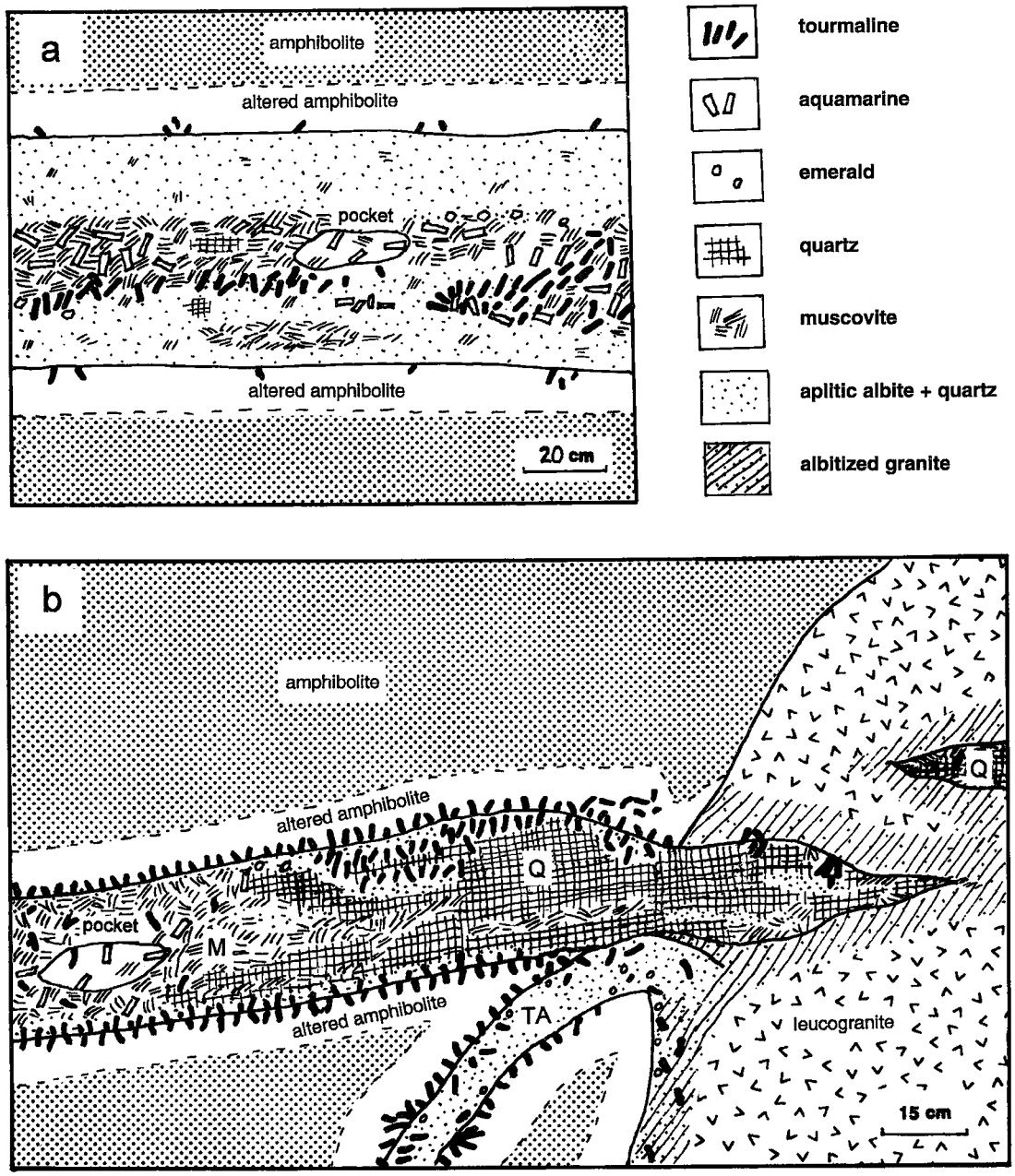

FIG. 8. Schematic mineralogy and texture of pegmatite and veins at Khaltaro. (a) Typical zoned albite-rich pegmatite. (b) Setting and character of hydrothermal veins, showing gradation of quartz vein (Q) laterally into muscovite vein (M); tourmaline–albite vein (TA) is gradational into albitized leucogranite.

pods up to 1 m thick. Although several types of pegmatite were recognized in the field, the most abundant and widespread are zoned albite-rich dikes (Fig. 8a). At Mine 1, these dikes contain an aplitic to medium-grained (<3 mm) outer zone that surrounds a discontinuous coarse-grained (1.5 to 2.5 cm) core zone. The outer zone is aplitic and albite-rich, with subordinate quartz and traces of muscovite and fluorite, and the core zone contains widely varying amounts of muscovite, quartz, and beryl, with local aggregates and sunbursts of tourmaline and traces of albite and fluorite. Pockets within the core zone contain euhedral crystals of pale aquamarine and platy albite (variety "cleavelandite"), with or without muscovite, dark brown tourmaline, and fluorite. The maximum dimension of the pockets rarely exceeds 30 cm. At the Mine 2 area, the zoned lenses of albite-rich pegmatite are texturally similar to the dikes at Mine 1, but the outer zone also contains traces of tourmaline and beryl. Muscovite is absent in the inner zone, which contains coarse albite (5 to 7 cm) and subordinate quartz, euhedral aquamarine (1.5 to 5 cm), and cross-cutting aggregates of prismatic tourmaline and quartz. Pockets within the core zone contain euhedral crystals of albite, pale aquamarine, and dark brown tourmaline. Emerald uncommonly forms within the pegmatites, as small (0.5 cm) anhedra within the fine-grained outer zone, or within the core of color-zoned aquamarine crystals along the pegmatite's outer core margin. As discussed below, the albite-rich assemblages in the pegmatites are interpreted to result from metasomatism.

Other pegmatite types are uncommon, and do not appear to contain emerald mineralization. In the Mine 1 area, a biotite-bearing pegmatite dike crops out for 7 m and is 40 cm wide (Fig. 3: unit P_{kpb}). Folding of the enclosing amphibolite has caused shearing in the pegmatite, which consists of coarse-grained (1 to 2.5 cm) partially albitized K-feldspar with subordinate plagioclase, quartz, and biotite, and traces of muscovite, arsenopyrite, and apatite. A weak zonation is defined by biotite near the margins and rare muscovite in the core. The pegmatite has been intruded by several subparallel veinlets of fine- to medium-grained quartz, albite, and tourmaline. An emerald-mineralized hydrothermal vein dominated by tourmaline and albite is present along one side of the pegmatite. Another variety of pegmatite is exposed in a shallow trench in the Mine 1 area, ~30 m southeast of the area mapped. It measures <1 m wide and at least 10 m long, and is composed of coarse-grained (<2 cm) albite (80%) and muscovite (20%), with vuggy areas containing albite intergrown with euhedral crystals of pale aquamarine, muscovite, and (rarely) cubes of pale pink fluorite showing (110) and (101) faces. Quartz and tourmaline are conspicuously absent from this albitized pegmatite. In the Mine 2 area, a small lens of coarse-grained

TABLE 5. AVERAGE TOURMALINE COMPOSITIONS (ELECTRON MICROPROBE) FROM PEGMATITE, VEINS, AND ALTERED AMPHIBOLITE, KHALTARO

	pegmatite (n=9)	vein (n=27)	Bt+Tur+Fl zone (n=10)
SiO_2 (wt%)	36.54±33	36.91±49	37.13±76
TiO_2	0.76±23	0.47±24	0.35±10
Al_2O_3	31.87±81	32.10±1.29	31.23±1.18
Cr_2O_3	0.03±5	0.15±21	0.13±11
V_2O_5	0.05±3	0.04±3	0.02±1
FeOT	10.45±1.48	8.16±1.51	6.39±79
MnO	0.15±12	0.23±17	0.14±11
NiO	0.02±3	0.03±3	0.03±3
ZnO	0.03±3	0.07±7	0.05±6
MgO	5.13±1.11	6.54±1.63	8.50±1.30
CaO	0.59±32	0.71±77	1.16±75
Na_2O	2.33±17	2.25±33	2.20±35
K_2O	0.05±1	0.04±2	0.04±1
SrO	0.00±0	0.00±0	0.00±0
Rb_2O	0.00±0	0.00±0	0.00±0
F	1.03±18	1.16±25	1.42±17
Cl	0.00±0	0.00±0	0.00±0
Sum	89.06±42	88.86±70	88.79±1.24
-O=F,Cl	0.44±8	0.49±11	0.60±7
$+(B_2O_3)$*	10.77	10.87	10.93
Total	99.40±42	99.24±65	99.12±1.22
Cations per 29 oxygen equivalents			
Si	5.896±22	5.903±50	5.906±34
Al	0.104±22	0.097±50	0.094±34
Tet. sum	6.000	6.000	6.000
Al (Z site)	5.923±76	5.887±189	5.747±195
Al	0.037±78	0.068±107	0.015±31
Mg	1.233±263	1.558±383	2.014±301
Fe	1.411±205	1.093±210	0.851±114
Ti	0.092±28	0.057±29	0.042±12
Mn	0.021±16	0.031±23	0.019±15
Cr	0.004±6	0.019±27	0.016±14
V	0.006±3	0.005±3	0.002±1
Ni	0.002±3	0.004±4	0.004±4
Zn	0.004±4	0.008±8	0.006±7
Sum Y	2.809±110	2.842±204	2.968±228
B*	3.000	3.000	3.000
Ca	0.103±57	0.121±133	0.197±127
Na	0.729±48	0.696±101	0.679±106
K	0.011±3	0.009±3	0.009±2
Sr	0.000±0	0.000±0	0.000±0
Rb	0.000±0	0.000±0	0.000±0
Sum X	0.843±38	0.827±71	0.885±36
F (pfu)	0.527±90	0.587±127	0.715±81
Cl (pfu)	0.002±2	0.002±1	0.000±0
Na/(Na+Ca)	0.88±6	0.86±14	0.78±14
Mg/(Mg+Fe)	0.46±9	0.58±10	0.70±6

* B is assumed present in stoichiometric proportion.
Error is one standard deviation of mean; n = number of analyses. O.S.U. Cameca SX-50 electron microprobe conditions: wavelength dispersive spectrometers; 15 kV accelerating voltage; 30 nA sample current; 3-5 μm beam diameter; computer PAP version of ZAF data reduction/correction; standardization at beginning and end for drift correction; detection limits 0.03-0.09 wt% oxide (except 0.13 for ZnO); counting errors (1σ) range from ±0.05 to ±0.2 wt% oxide. All Fe as FeO.

pegmatite about 1 m long and 30 cm wide was seen in a single exposure (Fig. 4: unit P_{atq}). This pegmatite forms along the border of a quartz vein, and is composed of uniformly coarse-grained (5 to 7 cm) blocky albite (70%), prismatic tourmaline (20%), and interstitial milky quartz (10%).

Hydrothermal veins

Hydrothermal veins consisting of quartz, muscovite, beryl, and tourmaline–albite are closely associated with the leucogranite and pegmatites (Fig. 8b). Electron-microprobe data for the tourmaline from the hydrothermal veins indicate that it is schorl (Table 5).

Quartz veins. Elongate bodies of quartz form (1) segregations and distinct lenses within the leucogranite, and (2) veins that grade from monomineralic to muscovite-rich (Fig. 8b), and that cross-cut amphibolite and garnet – mica schist. Other vein types cut and are cut by quartz veins, indicating that the quartz veins formed over a relatively wide time-interval. The quartz veins contain milky white quartz with local aggregates and vein-like masses of prismatic tourmaline, muscovite, albite, and beryl. These mineral aggregates may in turn be cracked and intruded by quartz. The widest lenses of quartz (1.6 m) appear to have resulted from multiple pulses of quartz deposition. Beryl within the quartz is typically translucent colorless or pale aquamarine, although fine crystals of emerald may be intergrown with quartz near the contacts of some veins [*i.e.*, at Mine 2: photo 3–24 of Kazmi *et al.* (1989)].

Muscovite veins. In proximity to the leucogranite, some quartz veins distally evolve into muscovite veins (Fig. 8b). More commonly, muscovite veins form within or near the leucogranite, as locally continuous veins up to 1 m thick. The veins contain coarse (2 cm) flakes of subhedral intergrown muscovite, with local translucent aquamarine, tourmaline, and interstitial albite. The muscovite veins are generally unzoned, but are locally flanked by thin borders of aplitic albite and quartz. The larger (>30 cm wide) muscovite veins are mined for aquamarine-bearing pockets. Emerald is rarely found in the core of aquamarine crystals near the contacts.

Beryl veins. In the Mine 2 area, uncommon veins of beryl up to 15 cm wide cross-cut the amphibolite (not shown on Fig. 8b). Beryl forms translucent, prismatic, pale blue to colorless crystals that are typically oriented perpendicular to the wallrock contacts. The beryl commonly forms compact aggregates of parallel crystals up to 5 cm long. Subordinate tourmaline, quartz, and fine-grained albite form interstitial fillings and irregular masses. Vuggy areas contain translucent to transparent euhedral aquamarine (<1 cm), "cleavelandite", and needles of dark brown tourmaline. No emerald was observed in these veins.

Tourmaline–albite veins. Narrow (<12 cm) tourmaline–albite veins contain medium- to coarse-grained tourmaline and aplitic albite and quartz, with accessory fluorite and apatite (Fig. 8b). The proportions vary over the complete range, from monomineralic tourmaline to monomineralic albite. The veins typically contain complex sheeted intergrowths of prismatic tourmaline (0.5 to 2 cm long) in fibrous mats and radiating sunbursts, which cut and are cross-cut by layers of granular albite and quartz. Less common are zoned veins containing albite-enriched margins and a tourmaline-enriched core. Quartz locally forms irregular masses and parallel veins enclosed by the tourmaline–albite veins. Vuggy areas contain wedge-shaped albite, crumbly needle-like tourmaline, and fluorite, with emerald locally. Vugs are rarely filled with calcite, which may enclose intergrown emerald and dark brown tourmaline along with local traces of talc. Emerald crystals are more commonly intergrown with granular albite and quartz than with tourmaline aggregates.

Other minerals are rarely found in the tourmaline–albite veins at Khaltaro. One vuggy specimen from the Mine 2 dump contains dark brown tourmaline needles in an earthy, rust-orange matrix, that is probably ralstonite (E.E. Foord, pers. comm., 1994). Rare, small (1 mm) crystals of subhedral allanite were seen within the aplitic outer margin of a tourmaline–albite vein. The allanite forms zoned pleochroic grains that contain abundant Cr (2.4–4.8 wt% Cr_2O_3), Ce (2.8–3.7 wt% CeO_2), and Th (3.2–5.3 wt% ThO_2) on the basis of electron-microprobe data. Titanite was noted in one specimen of aplitic albite and quartz collected from the tailings at Mine 2. The titanite forms small (1 mm) subhedral crystals intergrown with emerald.

Temporal and spatial relations of leucogranite, pegmatites, and veins

The intimate spatial relations and the gradational modal compositions of the leucogranite, pegmatites, and all veins suggest that they all formed during a single magmatic–hydrothermal event. The leucogranite is cut by both dikes of pegmatite and veins of muscovite, and the former appear to emanate from the leucogranite. Both pegmatites and veins characteristically taper or splay at their ends, where they grade into tourmaline–albite veins. The leucogranite is albitized in selvages adjacent to quartz and muscovite veins, which locally grade into one another. Tourmaline–albite veins emanate from albitized leucogranite, and cross-cut older veins and pegmatites. Thus, some early tourmaline–albite veins formed synchronously with pegmatites, whereas most postdate pegmatites and other vein types, which indicates a considerable time-interval of formation. Quartz veins

formed over a similar wide interval, since they cross-cut and are cross-cut by tourmaline–albite veins.

Crystal Chemistry of Beryl and Characteristics of Beryl from Khaltaro

Emerald is defined by the presence of Cr as the cause of color. Traces of V^{5+} also may cause the emerald-green color, and the relative proportion of Fe^{2+} to Fe^{3+} in different coordinations cause colors ranging from yellow to yellow-green to blue (Wood & Nassau 1968, Samoilovich *et al.* 1971). Aurisicchio *et al.* (1988) documented substitutions involving divalent and trivalent ions (Fe^{2+}, Mg^{2+}, Mn^{2+}, Fe^{3+}, Cr^{3+}, V^{5+}, and Sc^{3+}) as well as V^{5+} and Ti^{4+} for octahedrally coordinated Al, and also Li for tetrahedrally coordinated Be. Excess charge is balanced by the substitution of alkalis into the channel sites, by coupled substitutions such as: $^{[VI]}Al^{3+} + {}^{ch}\square \rightarrow {}^{[VI]}(Fe, Mg, Mn)^{2+} + {}^{ch}Na^{+}$, where ch = channel site and $\square$ = vacancy. Deer *et al.* (1992) reported that most of the Na resides in the channel site, along with H_2O.

The amount of Cr necessary to cause the emerald green coloration is indeed variable, and apparently depends on the environment of formation and accompanying impurities such as Fe. Garstone (1981) suggested that 0.14 to 0.50 wt% Cr_2O_3 is sufficient to produce the emerald green color in Australian emerald, and Fallick & Barros (1987) stated that >0.15 wt% Cr_2O_3 combined with traces of Fe and V results in dark green emerald at Porangatu, Brazil. Emerald-green color within variably zoned suture-related beryl crystals from Pakistan has been correlated with Cr (0.2 to 2.1 wt% Cr_2O_3) and, to a lesser extent, Fe, accompanied by variable Mg and Na (Hammarstrom 1989).

Emerald from Khaltaro may be distinguished from suture-related emerald in Pakistan by differences in cathodoluminescence emission spectra (Mariano 1987a), as well as greater amounts of Si and Al, and lesser amounts of Mg and Na in Khaltaro emerald (Hammarstrom 1989). Although Khaltaro emerald contains similar Si, Al, Fe, and Cr to emerald from quartz–carbonate veins at Panjshir, Afghanistan (Hammarstrom 1989), elevated Cs and relatively low contents of Sc, Fe, and Mg (Table 6) are consistent with the chemistry of beryl derived from granitic pegmatite (Staatz *et al.* 1965, Hammarstrom 1989).

Most of the gem-quality emerald production at Khaltaro has come from quartz and tourmaline–albite veins at Mine 2. According to local miners, fine euhedral crystals of emerald up to 2.5 cm long are found in "black dirt" (crumbly tourmaline?) in pockets within tourmaline–albite veins. The narrower (<20 cm) tourmaline–albite veins appear to host the most abundant mineralization. Emerald is less common in albitized leucogranite and in zoned albite-rich pegmatites. Regardless of its occurrence, emerald invariably forms adjacent to the host amphibolite, rarely more than 10 cm from the contact (Fig. 9). Within a given vein, emerald may form sporadically among closely associated pale blue and colorless beryl, as anhedral to subhedral crystals (0.5 to 1 cm long), which are typically intergrown with fine-grained albite,

TABLE 6. PARTIAL CHEMICAL COMPOSITIONS OF BERYL FROM PEGMATITE, VEINS, AND ALTERED AMPHIBOLITE, KHALTARO

Sample	32	19D	30B	33D1	33D2	Literature
Occurance	vein	peg	Bt+Tur +Fl zone	vein	vein	Khaltaro†
Color	colorless	pale blue	blue-green	light Em green	Em green	Em green
SiO_2 (wt.%)	66.77	66.87	66.54	66.61	66.14	64.80
TiO_2	0.00	0.00	0.00	0.00	0.00	0.01
Al_2O_3	18.54	18.46	17.02	16.19	15.57	17.10
Cr_2O_3	<0.01	<0.01	0.08	0.11	0.63	0.67
V_2O_5	0.00	0.00	0.00	0.01	0.03	0.04
FeOT	0.15	0.13	0.56	0.46	0.69	0.53
MnO	0.01	0.03	0.03	0.06	0.03	0.03
MgO	0.17	0.11	0.93	1.55	1.59	1.01
CaO	0.00	0.00	0.00	0.01	0.00	0.00
Na_2O	0.57	0.60	1.13	1.34	1.40	0.92
K_2O	0.00	0.02	0.01	0.05	0.06	n.d.
F	0.08	0.12	0.09	0.08	0.08	n.d.
Cl	0.00	0.00	0.00	0.00	0.00	n.d.
Sum	86.31	86.33	86.33	86.37	85.60	85.11
-O=F,Cl	0.03	0.05	0.04	0.03	0.03	n.d.
+(BeO*)	13.94	13.94	13.85	13.84	13.75	13.62
Total	100.22	100.22	100.14	100.18	98.76	98.73
Mg/(Mg+Fe)§	0.67	0.60	0.75	0.86	0.80	0.77
Sc (ppm)	5.93	14.1	95.2	83.4	93.9	70
Co	0.18	0.29	1.06	1.13	25.4	6
Ni	<84	<130	<570	<390	<330	40
Zn	41	42	<660	<450	<330	20
As	<8.1	<6.6	<33	<16	208	n.d.
Sb	<0.26	<0.42	<1.6	<0.96	<0.90	n.d.
Se	<11	<10	<39	<20	<19	n.d.
Rb	47	53	89	99	126	n.d.
Cs	1220	1220	2280	1920	2680	n.d.
Sr	<570	<510	<2300	<1900	544	10
Ba	<390	<250	<660	<720	<780	7
La	<0.23	<0.16	<0.66	<0.48	<0.42	<10
Ce	<13	<16	<33	<22	11.0	<20
Nd	<14	<18	<30	<42	<42	<20
Sm	n.d.	n.d.	n.d.	n.d.	0.13	n.d.
Eu	<0.09	<0.10	<0.39	<0.26	<0.21	<10
Tb	<0.66	<0.63	<2.4	<1.6	<1.2	n.d.
Yb	<1.6	<1.3	<2.4	<2.9	<2.7	<5
Lu	<0.20	<0.17	<0.30	<0.33	<0.45	n.d.
Hf	<1.7	<1.5	1.21	<3.9	<3.0	n.d.
Ta	0.22	<0.30	<0.87	<0.51	<0.57	n.d.
W	<3.0	<2.6	<18	<8.7	4.0	n.d.
Hg	<0.30	<0.30	<0.87	<0.63	<0.54	n.d.
Th	<2.6	<1.6	<9.0	<3.9	<3.6	<20
U	<4.2	<3.0	<12	<7.5	<9.0	<500

Major elements by electron microprobe; Cr_2O_3 and trace elements analyzed by INAA; INAA detection limits are elevated by varying amounts, due to a high Compton continuum produced by abundant Cs.
* BeO calculated by stoichiometry assuming 3 Be per 18 oxygen.
† Major element oxides averaged from 13 analyses by EPMA (Hammarstrom 1989); trace elements analyzed on representative sample by ICAP-AES; include Li=770 ppm and B=30 ppm (Snee *et al.* 1989).
§ molar proportions

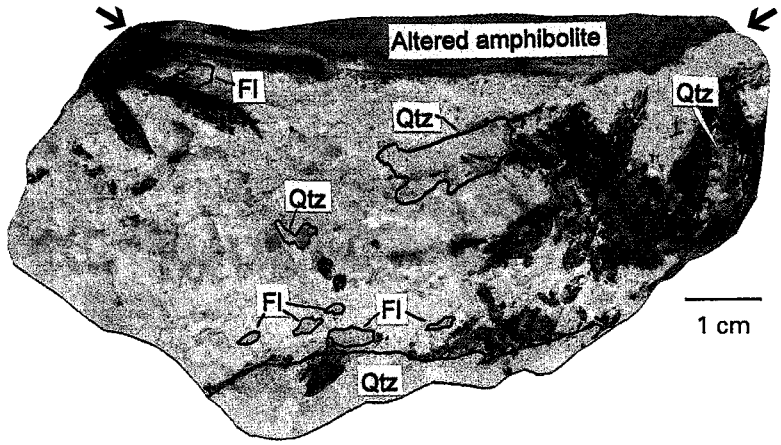

FIG. 9. Photograph of pale green emerald intergrown with aplitic-textured albite and quartz, black tourmaline, and fluorite in a hydrothermal vein from Mine 2. Specimen collected from the hanging-wall contact of a 25-cm-thick quartz vein, which locally contains a thin margin of aplite along the wallrock contacts. Emerald was seen in both the aplitic and quartz-rich portions of the vein. Arrows mark the contact with altered amphibolite.

quartz, and fluorite. The emerald crystals are typically unmodified hexagonal prisms with basal pinacoids; they are translucent, pale to medium green, and contain abundant fine cracks and inclusions. Microscope and microprobe examination of the mineral inclusions indicate that they consist of fluorite, albite, Mg-rich biotite (Table 7), and green chromian muscovite (Table 8). Rarely, the emerald contains abundant microscopic hollow tubes running parallel to the *c* axis, causing chatoyancy. Facet-grade emerald is rare, and confined to clear areas between cracks in some of the larger stones (Photo 3.24, Kazmi *et al.* 1989).

Where vein mineralization is particularly abundant, emerald also forms (rarely) in the altered amphibolite adjacent to the veins. This emerald forms subhedral to euhedral crystals within 5 cm of the vein contacts, where it is hosted by foliated aggregates of metasomatic magnesian biotite, fluorite, and tourmaline. Although the wallrock-hosted emerald does not contain any more mineral inclusions than vein-hosted emerald, the overall milky appearance of the crystals limits their gem potential.

Khaltaro beryl ranges in color, from colorless, to pale blue (aquamarine) and green, to the characteristic emerald green. All colors may be seen in a single crystal, as an emerald core grading into a colorless rim. Results of microprobe analyses along a traverse from a colorless rim to an emerald core show that the emerald portion is relatively enriched in Mg, Na, Fe, and Cr (Fig. 10), with corresponding low contents of Al. In this crystal, the emerald-green color is perceived only where Cr_2O_3 is at least 0.44 wt%, and FeO is at least 0.54 wt%. The pale green portion of the crystal contains somewhat less Cr (0.25 wt% Cr_2O_3) than emerald, and variable Fe (0.04–0.43 wt% $Fe_2O_3^T$). The colorless rim contains no detectable Cr, and minor Fe (0.07–0.18 wt%). Mariano (1987a) reported similar Cr contents for Khaltaro emerald (0.4 wt% Cr_2O_3); cocrystallized colorless beryl was found to contain less than 50 ppmw Cr_2O_3, which is sufficient to cause brilliant red cathodoluminescence. In contrast, colorless beryl from several other world localities show no Cr^{3+}-activated luminescence (Mariano 1987a).

Chemical analyses of unzoned crystals of beryl of varying colors reveal the same chemical trends according to color as analyses of the single zoned crystal (Table 6; Laurs 1995). Of the samples analyzed, emerald-green varieties contain 0.20–1.27 wt% Cr_2O_3 and 0.62–0.89 wt% $Fe_2O_3^T$; V is below the detection limit (0.08 wt% V_2O_5). Aquamarine and pale green beryl contain less $Fe_2O_3^T$ (0.10–0.63 wt%), and Cr is near or below the detection limit (0.07 wt% Cr_2O_3). Colorless beryl likewise contains no detectable Cr, and $Fe_2O_3^T$ ranges from 0.07 to 0.28 wt%. All of the beryl samples in Table 6 contain abundant Cs (>1200 ppm). In addition, substantial amounts of Sr (544 ppm) and As (208 ppm) were detected in the darkest emerald.

METASOMATISM OF THE AMPHIBOLITE

Identical alteration-induced assemblages are found adjacent to pegmatites, veins, and albitized leucogranite, but no metasomatism of amphibolite was seen adjacent to leucogranite that was not albitized. From the contact outward, a zoned selvage typically contains (1) a sporadic inner Biotite – Tourmaline – Fluorite

TABLE 7. REPRESENTATIVE BIOTITE COMPOSITIONS (ELECTRON MICROPROBE) FROM LEUCOGRANITE, PEGMATITE, INCLUSIONS IN EMERALD, AND ALTERED AMPHIBOLITE, KHALTARO

Sample #	25	24	17A	17C1	17C2	17C3
Occurrence	lgr	peg	Tur>Ab vein inclus in Em	alt'd amph Bt+Tur +Fl	alt'd amph Bt+Ab +Fl	alt'd amph sparse Bt+Qtz
Description	Bt-rich	Kfs+Ab +Bt				
SiO_2 (wt%)	36.52	35.89	43.77	42.36	41.06	36.52
TiO_2	2.69	2.31	1.21	0.46	0.64	0.89
Al_2O_3	17.35	15.80	12.93	12.88	13.51	17.39
Cr_2O_3	0.01	0.00	0.19	0.12	0.10	0.11
V_2O_5	0.00	0.03	0.04	0.02	0.05	0.00
FeO^T	22.17	24.64	8.68	12.41	15.56	19.35
MnO	0.29	0.29	0.26	0.31	0.33	0.30
MgO	7.85	8.55	19.19	17.48	15.28	11.69
CaO	0.00	0.00	0.02	0.02	0.00	0.02
Na_2O	0.02	0.06	0.15	0.06	0.12	0.18
K_2O	9.72	9.33	9.63	9.11	9.34	8.65
BaO	0.00	0.08	0.00	0.00	0.03	0.02
Rb_2O	0.12	0.15	0.37	0.40	0.33	0.36
F	1.86	2.14	5.36	4.68	3.90	2.18
Cl	0.00	0.02	0.00	0.00	0.04	0.03
Sum	98.61	99.30	101.81	100.29	100.30	97.68
-O=F,Cl	0.78	0.91	2.26	1.97	1.65	0.93
$+(H_2O)^*$	3.14	2.97	1.91	2.10	2.38	3.00
Total	100.96	101.36	101.46	100.42	101.03	99.76
Cations per 22 oxygen equivalents						
Si	5.448	5.395	5.889	5.882	5.804	5.414
Al	2.552	2.605	2.051	2.108	2.196	2.586
Tet. sum	8.000	8.000	7.941	7.989	8.000	8.000
Al	0.499	0.196	0.000	0.000	0.055	0.452
Mg	1.745	1.917	3.849	3.617	3.220	2.583
Fe	2.766	3.097	0.976	1.440	1.839	2.399
Ti	0.301	0.261	0.122	0.048	0.068	0.099
Mn	0.037	0.037	0.029	0.036	0.039	0.037
Cr	0.002	0.000	0.021	0.014	0.011	0.012
V	0.000	0.002	0.003	0.001	0.005	0.000
Oct. sum	5.350	5.511	4.942	5.146	5.237	5.582
Ca	0.001	0.000	0.003	0.003	0.000	0.003
Na	0.005	0.017	0.039	0.015	0.032	0.051
K	1.849	1.789	1.652	1.614	1.684	1.635
Ba	0.000	0.004	0.000	0.000	0.001	0.000
Rb	0.011	0.015	0.032	0.035	0.030	0.035
Int. sum	1.868	1.826	1.726	1.668	1.748	1.725
F (pfu)	0.878	1.019	2.281	2.053	1.745	1.023
Cl (pfu)	0.001	0.006	0.000	0.000	0.010	0.008
Mg/(Mg+Fe)	0.39	0.38	0.80	0.72	0.64	0.52
Al/(Al+Si)	0.36	0.34	0.26	0.26	0.28	0.36

Abbreviations: altered, alt'd; leucogranite, lgr; pegmatite, peg; amphibolite, amph; inclusion, inclus; emerald, Em.
* H_2O is calculated by stoichiometry.

TABLE 8. REPRESENTATIVE MUSCOVITE COMPOSITIONS (ELECTRON MICROPROBE) FROM LEUCOGRANITE, VEINS, INCLUSIONS IN EMERALD, AND ALTERED AMPHIBOLITE, KHALTARO

Sample #	27	26F	28B	33C2	28D1
Occurrence	lgr	Ms-rich vein	Ab>>Tur vein	aplitic vein	alt'd amph
Description	albitized	coarse flakes	aplite	inclus in Em	Bt+Tur +Fl zone
SiO_2 (wt%)	48.23	47.41	48.48	48.88	48.58
TiO_2	0.48	0.26	0.14	0.08	0.27
Al_2O_3	29.82	30.82	30.59	29.47	28.92
Cr_2O_3	0.00	0.01	0.06	1.64	0.04
V_2O_5	0.03	n.d.	0.00	0.00	n.d.
FeOT	2.67	2.41	2.40	1.57	2.17
MnO	0.15	0.20	0.22	0.09	0.34
MgO	1.65	1.93	2.20	2.41	2.73
CaO	0.00	0.01	0.02	0.00	0.00
Na_2O	0.26	0.27	0.21	0.23	0.19
K_2O	10.64	10.55	9.51	10.49	10.58
BaO	0.26	0.14	0.22	0.19	0.11
Rb_2O	0.19	0.32	0.14	0.22	0.26
F	1.99	1.68	1.64	1.34	2.09
Cl	0.00	0.00	0.02	0.00	0.00
Sum	96.38	96.01	95.84	96.62	96.28
-O=F,Cl	0.84	0.71	0.70	0.56	0.88
$+(H_2O)^*$	3.56	3.69	3.74	3.89	3.52
Total	99.10	98.99	98.89	99.95	98.92
Cations per 22 oxygen equivalents					
Si	6.426	6.337	6.431	6.474	6.466
Al	1.574	1.663	1.569	1.526	1.534
Tet. sum	8.000	8.000	8.000	8.000	8.000
Al	3.109	3.193	3.215	3.076	3.004
Mg	0.327	0.384	0.436	0.475	0.542
Fe	0.297	0.269	0.266	0.174	0.242
Ti	0.048	0.026	0.014	0.008	0.027
Mn	0.017	0.023	0.024	0.010	0.038
Cr	0.000	0.001	0.006	0.172	0.004
V	0.003	0.000	0.000	0.000	0.000
Oct. sum	3.801	3.896	3.961	3.915	3.857
Ca	0.000	0.002	0.003	0.000	0.000
Na	0.068	0.070	0.054	0.059	0.050
K	1.808	1.798	1.609	1.773	1.797
Ba	0.014	0.007	0.011	0.010	0.006
Rb	0.016	0.028	0.012	0.019	0.023
Int. sum	1.906	1.904	1.689	1.861	1.875
F (pfu)	0.839	0.710	0.689	0.560	0.878
Cl (pfu)	0.000	0.000	0.004	0.000	0.000
Mg/(Mg+Fe)	0.52	0.59	0.62	0.73	0.69
Al/(Al+Si)	0.42	0.43	0.43	0.42	0.41

* H_2O is calculated by stoichiometry.

zone 2 to 3 cm wide, (2) an intermediate Biotite – Plagioclase – Fluorite zone 7 to 8 cm wide, and (3) an outer Sparse Biotite zone 10 cm wide (Figs. 11, 12). The three zones must have developed contemporaneously in response to chemical gradients, because they are consistently developed in the same progressive

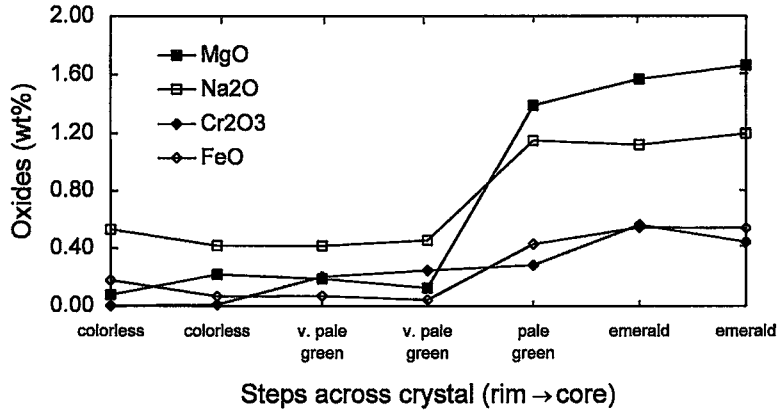

FIG. 10. Results of electron-microprobe analyses from rim to core (11-mm traverse) across a color-zoned crystal of beryl.

metasomatic sequence outward from the contacts, and the inner zones do not cross-cut unaltered amphibolite. The selvages are up to 30 cm wide (typically <20 cm wide), and locally penetrate over 1 m along fractures. Visual modifications are typically confined to a distance that is less than half the width of the associated vein, although large variations occur. The most intense metasomatism appears to be developed next to muscovite or quartz veins, especially those that show multiple episodes of vein formation.

Biotite – Tourmaline – Fluorite zone

The inner Biotite – Tourmaline – Fluorite zone forms a discontinuous selvage adjacent to the pegmatites or veins, and is characterized by metasomatic aggregates of biotite, tourmaline, and fluorite, with or without muscovite, albite, quartz, and beryl. Alteration has completely recrystallized the amphibolite, leaving no trace of the pre-existing minerals or textures (Fig. 11). The Biotite – Tourmaline – Fluorite zone typically extends up to 3 cm outward from the contact, but is sporadic in occurrence and intensity. In places (*e.g.*, near veins containing abundant muscovite), the zone is pervasively developed, with isolated sunbursts of tourmaline forming >12 cm from the contacts. The distal margin of the zone is gradational, and defined by the last appearance of tourmaline. Not included in this zone are metasomatic tourmaline and albite that form along fractures extending up to 0.5 m from the contact.

The metasomatic minerals occur in widely varying proportions (Fig. 12). Tourmaline forms subhedral prismatic crystals up to 2 cm long that radiate outward from the contact. Fluorite, quartz and albite ($<An_6$) forms small (0.1 to 1.0 mm) disseminated grains and locally abundant inclusions within tourmaline. Biotite and muscovite form medium- to coarse-grained (<5 mm), randomly oriented and foliated aggregates that form interstitial to the tourmaline sprays. Biotite commonly hosts fluorite inclusions along cleavage planes. The metasomatic biotite is Mg-rich [typical molar Mg/(Mg + Fe) in the range 0.60 to 0.70: Laurs 1995], and is hereafter referred to simply as biotite.

Sporadic disseminations and accumulations of beryl rarely form in the Biotite – Tourmaline – Fluorite zone adjacent to veins containing abundant beryl. The metasomatic beryl typically forms translucent to transparent, emerald green to blue-green, anhedral to euhedral crystals (<1.5 cm long), that are intergrown with biotite, tourmaline, albite and fluorite.

Biotite – Plagioclase – Fluorite zone

Outward from and adjacent to the Biotite – Tourmaline – Fluorite zone is a ubiquitous zone characterized by metasomatic aggregates of biotite, plagioclase, fluorite, and local quartz. Compared to the Biotite – Tourmaline – Fluorite zone, the amount of plagioclase and quartz increases, and that of fluorite decreases (Fig. 12). Plagioclase and local quartz form fine-grained (<1.3 mm) disseminations and irregular aggregates within biotite. The biotite gradually decreases in grain size (5 to 2.5 mm) away from the contact (Fig. 11). The mineralogy and texture of original amphibolite may be recognized within 0.5 cm of the outer edge of the Biotite – Plagioclase – Fluorite zone, where relict amphibole is partially replaced by biotite along fractures and cleavages, and the zoisite is partially altered to optically continuous plagioclase with sparse inclusions of biotite. Metasomatic plagioclase is differentiated from metamorphic (relict)

plagioclase by its fine grain-size and its association with quartz or location within former grains of zoisite. Incipient alteration of garnet was not observed, owing to the scarcity of garnet in the amphibolite samples.

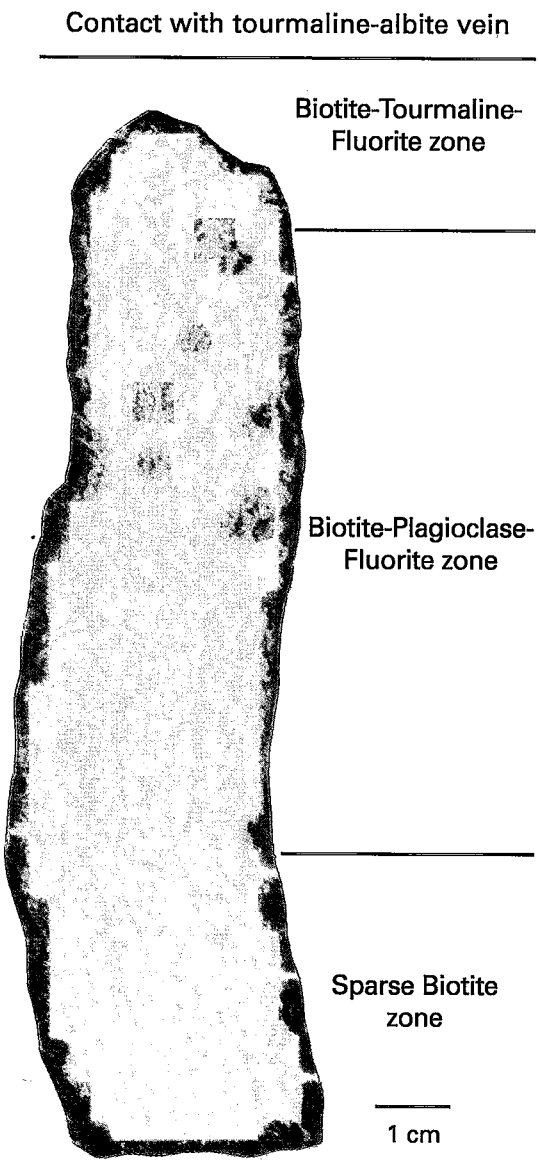

FIG. 11. Photograph of half of a symmetrically zoned amphibolite selvage (sample 17C) adjacent to a tourmaline–albite vein, Mine 2. Approaching the vein contact, the dark green Sparse Biotite zone, with relict amphibole and garnet, grades into the light brown Biotite – Plagioclase – Fluorite zone, which abruptly grades into the darker Biotite – Tourmaline – Fluorite zone. The vein contact is ~1 cm from the end of the sample.

Sparse Biotite zone

In the distal alteration assemblage, sparse amounts (<5%) of biotite and local traces of quartz coexist with minerals relict from the original metamorphic amphibolite assemblage. The distal extent of the Sparse Biotite zone is not well established, owing to the variable thickness of this zone and its gradational nature. Relict plagioclase and zoisite appear unaffected by metasomatism in the Sparse Biotite zone. Quartz forms elongate blebs and rare cross-cutting veinlets containing biotite and local plagioclase. Biotite also forms coarse poikiloblastic overgrowths and preferentially replaces fine-grained amphibole that forms premetasomatic rims around garnet porphyroblasts. The biotite is commonly chloritized.

Mineral chemistry

Electron-microprobe analyses of tourmaline, biotite, muscovite, and plagioclase record systematic variations in mineral chemistry with increasing distance from the contact; results are summarized in Figure 13.

Tourmaline. Average molar Mg/(Mg + Fe) value of the tourmaline is 0.70 (Table 5, Fig. 13), which is thus schorl-dravite. Zoning within single crystals is inconsistent, even within the same thin section. The pleochroic color in plane-polarized light ranges from blue-olive to brown-olive, in irregular or concentric zones (perpendicular to the *c* axis), which commonly repeat. The blue varieties contain slightly more Fe, but Mg, Ca, and Na show no consistent correlation with color. Rb, Sr, and Cl were not detected, but F is relatively high (1.4 wt%). Compared with tourmaline from the associated pegmatites and veins, elevated contents of Mg, Ca, and Cr in exomorphic tourmaline (Table 5) are consistent with derivation of these components from the amphibolite. The molar Mg/(Mg + Fe) value of the metasomatic tourmaline is similar to that of the amphibolite.

Biotite and Muscovite. With increasing distance from the contact, the biotite shows evidence of minor increases in Ti, ^{IV}Al, and Na, and decreases in Si and F (Table 7). The slight enrichment in ^{IV}Al and Na in biotite away from the contact may be due to preferential incorporation of these elements into coexisting tourmaline and plagioclase within the inner alteration zones. The molar Mg/(Mg + Fe) value of biotite is highest in the inner zones, and decreases progressively away from the contact (Table 7, Fig. 13). This trend may result from preferential leaching of Fe over Mg in the F-rich hydrothermal fluids; whole-rock analyses of the Biotite – Tourmaline – Fluorite zone in sample #17C indicate that approximately 30 mol.% Fe and 20 mol.% Mg have been removed (Fig. 14). Foord *et al.* (1986) likewise documented greater removal of Fe than Mg from gabbro adjacent to granitic pegmatite

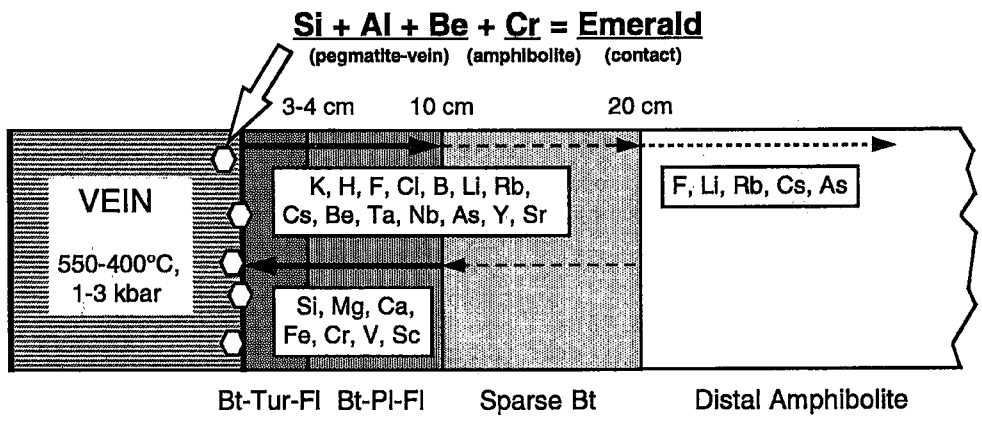

	Bt-Tur-Fl	Bt-Pl-Fl	Sparse Bt	Distal Amphibolite
Tourmaline	3-50	0	0	0
Biotite	10-90	35-70	tr-5	0-tr
Fluorite	2-20	tr-10	0	0
Na-Plagioclase	0-20	3-35	0	0
Quartz	0-8	0-20	tr-5	0
Relict minerals	none	±Hbl, ±Zo	Hbl, Pl, Zo, Ga	Hbl, Pl, ±Zo, ±Ga

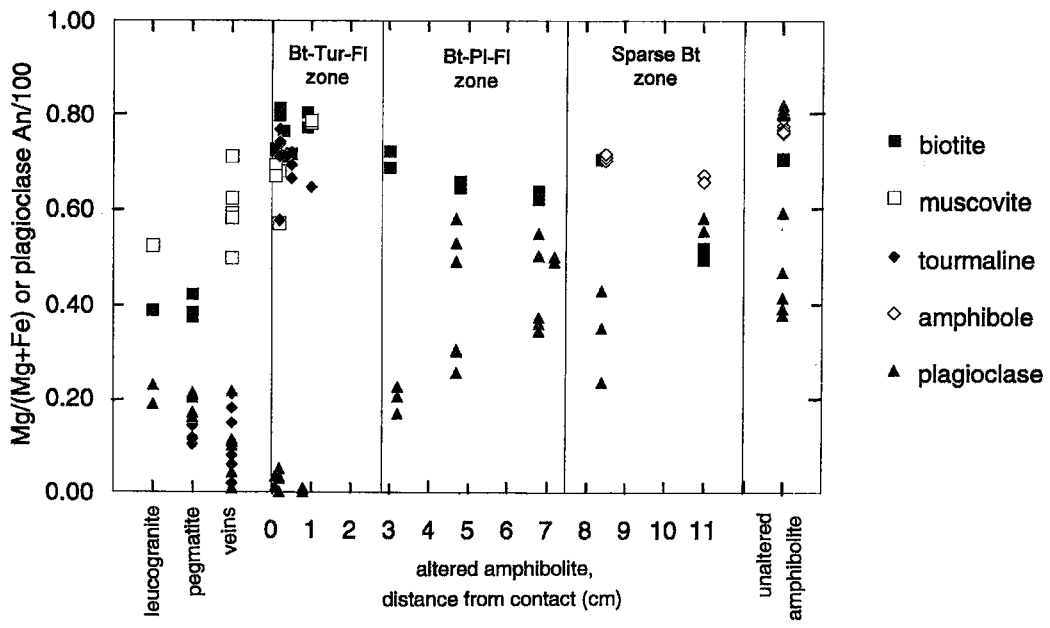

FIG. 12. Schematic diagram of half of a symmetrically zoned amphibolite selvage adjacent to a pegmatite or hydrothermal vein, showing addition and subtraction of components between pegmatite or hydrothermal vein and surrounding amphibolite. Modal data (volume %) are estimated from thin sections. Emerald forms within the vein, near the contact with the altered amphibolite.

in San Diego County, California.

Compared to biotite in pegmatite, the exomorphic biotite at Khaltaro is enriched in F (up to 4.7 wt%) and Rb (0.40 wt% Rb_2O) (Table 7), which reflects the migration of these incompatible elements out of the pegmatite–vein system. Cs (not determined by microprobe) is presumed present in the exomorphic micas, since significant amounts are detected in whole-rock analyses of the altered amphibolite (up to 890 ppm: Table 9).

Exomorphic muscovite is locally intergrown with tourmaline sprays. The muscovite is pale to medium green, with gradational contacts into the surrounding bronze biotite. The green color seems to be caused by relatively high amounts of Mn combined with Fe (Table 8: #28D1). Cr is insignificant in the muscovite, but is enriched in the biotite (0.12 wt%).

Plagioclase. The sodic composition ($An_{<6}$) of plagioclase near the contacts (Fig. 13) may be due to late-stage, low-temperature fluids associated with albitization of the pegmatites and veins, which were channeled along the contact with the altered amphibolite. The An-content of plagioclase gradually increases away from the contact (Fig. 13); within the Biotite – Plagioclase – Fluorite zone, the composition ranges from An_{17} to An_{60}, with a sodic rim that is enriched by ~20 mol.% albite over the coexisting core.

Whole-rock geochemistry

Gains and losses of major and trace elements in metasomatized amphibolite were determined at varying distances from the pegmatites and veins. Individual samples up to 20 cm long were divided into two or three portions for analysis, allowing observation of chemical variations within each alteration zone. The amount of major elements gained or lost from the altered amphibolite (in μmol element/g sample) was calculated using a constant-volume assumption, by normalizing chemical composition to specific gravity, as presented by Kretz *et al.* (1989) after Gresens (1967). Constant volume during metasomatism is supported by the lack of increased porosity and by the absence of any deflection of foliation trends within the alteration selvages.

Major-element variations in the altered amphibolite show enrichment in K and removal of Si, Mg, Fe, and Ca. Al and Na show slight, inconclusive gains and losses. The trends observed in a single traverse of the wallrock (Table 9, Fig. 14a) generally agree with trends observed in scattered samples of altered amphibolite from throughout the field area (Fig. 14b). Some chemical variation is expected in these scattered samples, due to premetasomatic chemical fluctuations (*cf.* standard deviations in Table 2). Significant chemical exchange has occurred only within the inner Biotite – Tourmaline – Fluorite zone and the intermediate Biotite – Plagioclase – Fluorite zone. The Sparse Biotite zone shows slight to imperceptible gains and losses of major elements following the patterns observed in the inner and intermediate zones. The net loss in major-element oxides for strongly altered samples is partly balanced by gains in F and B.

Owing to large variations of initial trace-element contents in the amphibolite, chemical exchange of these elements must be evaluated with caution. Gains and losses were evaluated by the consistency of changes in the concentration of each element within a single traverse of the wallrock (Table 9, Fig. 15). Cr, V, and Sc show notable depletion within the Biotite – Tourmaline – Fluorite zone. Substantial enrichment of F, Li, Rb, and Cs has occurred in all alteration zones, even within the distal Sparse Biotite zone (Table 9). Gains of Li, Rb, and Cs are likely greater than perceived in Figure 15, because small amounts of these highly mobile elements infiltrated the "unaltered" sample that was used for comparison (*cf.* Table 9: Li, Rb, and Cs contents of #17F). Enhanced amounts

FIG. 13. Electron-microprobe data concerning minerals occurring in leucogranite, pegmatite, veins, and amphibolite.

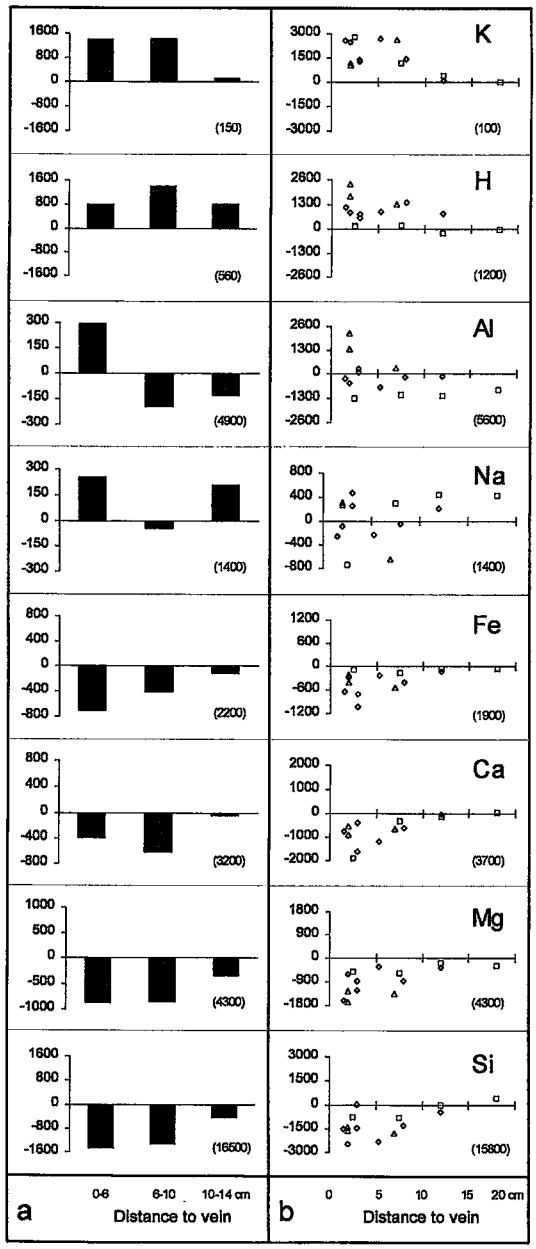

FIG. 14. Major-element gains and losses (in μmol/g, using a constant-volume assumption) in altered amphibolite, plotted against distance from hydrothermal veins. From the contact outward, the alteration zones typically extend 0–3 cm for the Biotite – Tourmaline – Fluorite zone, 3–10 cm for the Biotite – Plagioclase – Fluorite zone, and 10–20 cm for the Sparse Biotite zone. Graphs show: (a) single wallrock traverse (sample 17C: Table 8) adjacent to a tourmaline–albite vein, and (b) scattered samples from throughout the field area, adjacent to quartz veins (□), tourmaline–albite veins (◊), and muscovite veins (Δ). Numbers in parentheses are element abundances (μmol/g) in unaltered amphibolite for comparison, (a) in proximity to sample 17C, and (b) averaged from five scattered samples.

of F (Table 9) occur in both the fluorite-bearing inner and intermediate zones, and of B in the inner Biotite – Tourmaline – Fluorite zone. Modest concentrations of Be gradually diminish outward across the selvage. Both Y and Sr are enriched only in the inner Biotite – Tourmaline – Fluorite zone. The *HFSE* Ta and Nb are slightly enriched in the proximal zones, but not distally. Arsenic is enriched by nearly the same amount in all alteration zones. The *REE* show small, indeterminate variations.

Whole-rock analysis of a narrow (<8 cm) vein composed of tourmaline (~80 vol.%), albite (~15%), quartz (3%) and fluorite (1%) shows enrichment in Mg, Ca, Fe, Cr, and Ni (Table 9: #17A). These elements are not expected in such high concentrations in evolved B- and F-rich hydrothermal fluids, and were therefore likely derived from the amphibolite and incorporated into tourmaline and fluorite within the vein. Mass-balance calculations could not be made between the altered amphibolite series and the vein sample in Table 9, because the amphibolite was not obtained adjacent to this vein. Whole-rock chemical analyses were not determined for the pegmatites, owing to the difficulty in obtaining representative samples of such coarse-grained, heterogeneous bodies.

OXYGEN ISOTOPES

A reconnaissance oxygen isotopic study was performed on 20 mineral separates from the garnet–mica schist, amphibolite, altered amphibolite, leucogranite, pegmatite, and veins (Table 10). Analytical procedures are noted in Table 10. The garnet–mica schist contains muscovite with $\delta^{18}O$ = 8.8‰, and quartz with $\delta^{18}O$ = 12.3‰. Hornblende from the amphibolite yielded $\delta^{18}O$ = 6.6‰, and plagioclase $\delta^{18}O$ varies from 7.8 to 9.2‰, which is slightly greater than the $\delta^{18}O$ value expected of typical basaltic and andesitic magmas (6.5 ± 1‰; Taylor 1979). The fluids that formed the pegmatite–vein system have isotopically perturbed the adjacent altered amphibolite. Within a distal sequence of amphibolite adjacent to a quartz vein, plagioclase is isotopically heavier nearer to the vein by 1.6‰ (26D3 *versus* 26D4,

TABLE 9. GEOCHEMISTRY OF A TOURMALINE-ALBITE VEIN AND AN ALTERED AMPHIBOLITE SERIES, KHALTARO

Sample #	17A	17C1	17C2	17C3	17F
Description	Tur-Ab-Fl Vein	Bt-Tur-Fl	Bt-Pl-Fl	Sparse Bt+Qtz	unaltered
Dist. to vein		0-6 cm	6-10 cm	10-14 cm	3.6 m
SiO_2 (wt%)	46.18	48.53	49.73	50.56	50.77
TiO_2	0.21	0.33	0.39	0.45	0.42
Al_2O_3	28.42	16.18	14.90	14.52	14.57
Fe_2O_3T	5.78	7.02	8.56	9.61	9.97
MnO	0.10	0.15	0.18	0.20	0.22
MgO	6.55	8.49	8.66	9.54	10.13
CaO	4.32	9.74	9.12	10.66	10.57
Na_2O	4.24	3.06	2.53	2.90	2.46
K_2O	0.57	4.49	4.65	0.73	0.42
P_2O_5	0.12	0.03	0.03	0.03	0.04
LOI	3.05	1.49	2.18	1.49	0.59
Σ wt.%	99.54	99.51	100.92	100.69	100.16
Sc (ppm)	13.7	20.5	35.4	41.2	42.0
V	173	112	282	324	337
Cr	571	158	583	699	688
Ni	151	538	167	244	200
Cu	33	62	28	75	92
Zn	105	151	70	73	78
Ga	37	15	13	12	12
As	54.1	143	98	125	21
Sb	0.14	0.10	<0.42	0.23	0.14
Se	2.4	3.7	<6.3	<3.9	<3.3
F	7300	>10000	>10000	5300	750
B	>10000	1740	40	25	10
Be	48	180	95	45	1.0
Li	190	1150	1100	275	155
Rb	158	82	1359	142	38
Cs	34.1	667	890	90.5	21.9
Sr	115	1330	40	27	88
Ba	35	<24	67	<24	<24
La	1.7	1.5	1.5	1.3	1.1
Ce	5.1	<7.5	<9.3	<5.7	2.7
Nd	3.4	<130	<11	5.8	3.0
Sm	0.64	0.83	0.98	0.98	0.81
Eu	0.18	0.36	0.59	0.45	0.35
Tb	0.16	0.24	0.28	0.33	0.27
Yb	0.59	1.10	1.40	1.52	1.50
Lu	0.10	0.21	0.20	0.24	0.24
Y	10	58	<1	13	14
Zr	<1	4	3	6	6
Hf	0.55	0.44	0.52	0.52	0.61
Nb	4	17	7	1	1
Ta	1.79	1.94	0.67	<0.21	0.07
Hg	<0.10	<0.30	<0.39	<0.24	<0.21
Tl	<10	<10	<10	<10	<10
Th	<0.07	0.8	<1.2	<1.3	<1.2
U	<1.7	<4.2	<5.4	<3.9	<3.6

Note: Samples 17A and 17C are not adjacent samples.

Table 10). Conversely, biotite becomes progressively lighter adjacent to a tourmaline–albite vein. A compositional effect caused by increasing Mg/(Mg + Fe) toward the contact would result in isotopically heavier values of biotite (*cf.* O'Neil 1986), which contradicts the measured shift. Temperature variations should not cause the shift in $\delta^{18}O$ values of biotite, because biotite–water fractionation remains unchanged over a wide interval of temperature (Bottinga & Javoy 1973). Therefore, the isotopic shift in biotite adjacent to a tourmaline–albite vein may be caused by isotopic equilibrium between the biotite and coexisting metasomatic quartz and plagioclase, the latter two being relatively enriched in ^{18}O.

Uniformly high mineral $\delta^{18}O$ values from the leucogranite (quartz: 12.0‰), and a pegmatite (quartz: 10.7‰) support derivation by anatexis of supracrustal rocks (*cf.* Longstaffe 1982). Quartz veins have similar high $\delta^{18}O$ values (12.1 to 12.2‰), suggesting formation of the pegmatite–vein system by a single magmatic fluid derived from the leucogranite. Calculated $\delta^{18}O$ values of H_2O in equilibrium with coexisting mineral pairs (see below) at 400 to 500°C are 9.0‰ for leucogranite, 8.4‰ for pegmatite, and 7.4‰ for a quartz vein. All these H_2O values fall within $\delta^{18}O$ range of magmatic fluids. Progressively lighter $\delta^{18}O$ H_2O values in the order leucogranite → pegmatite → vein probably reflect increasing interaction over time of fluid with the isotopically lighter amphibolite wallrock, as well as decreasing temperature of the fluid.

TABLE 10. OXYGEN ISOTOPE DATA FOR MINERALS FROM MICA SCHIST, AMPHIBOLITE, LEUCOGRANITE, PEGMATITE, AND VEINS, KHALTARO

Sample #	Description	Mineral	$\delta^{18}O$, ‰
MICA SCHIST			
16	unaltered	Ms	8.8
"	"	Qtz	12.3
AMPHIBOLITE			
15B	unaltered	Hbl	6.6
"	"	Pl (An_{25})	9.2±0.2
26D4	unaltered, 23 cm from vein	Pl	7.8
ALTERED AMPHIBOLITE			
17C1	Bt+Tur+Fl zone, 0-6 cm	Bt	7.7±0.7
17C2	Bt+Pl+Fl zone, 6-10 cm	Bt	8.0±0.1
17C3	sparse Bt zone, 10-14 cm	Bt	8.4±0.4
26D3	sparse Bt zone, 14-21 cm	Pl	9.4
LEUCOGRANITE			
25	porphyroblastic	Qtz	12.0
"	"	Pl (An_{20})	10.0
27	albitized	Ms	9.1
PEGMATITE			
19A	zoned, albite-rich	Qtz	10.7
"	"	Pl (An_{22})	10.4
"	"	Ms	9.0
VEINS			
34	Mus-rich, +aquamarine	Ms	9.8
17D	Qtz>>Tur+Pl+Em	Qtz	12.1
"	"	Pl (An_3)	9.6
"	"	Em	10.7
23B	Qtz lens; no Em	Qtz	12.2

Analyses performed at O.S.U. using CO_2-laser to heat 2 to 5 mg sample to 2000°C, reaction with ClF_3 reagent, and conversion to CO_2; extraction line design modified after Sharp (1990). Data are reported as permil (‰) relative to V-SMOW. Analyses of NBS-28, NBS-30, & NCSU standards yield ±0.2‰ precision. Error is one standard deviation based on replicates.

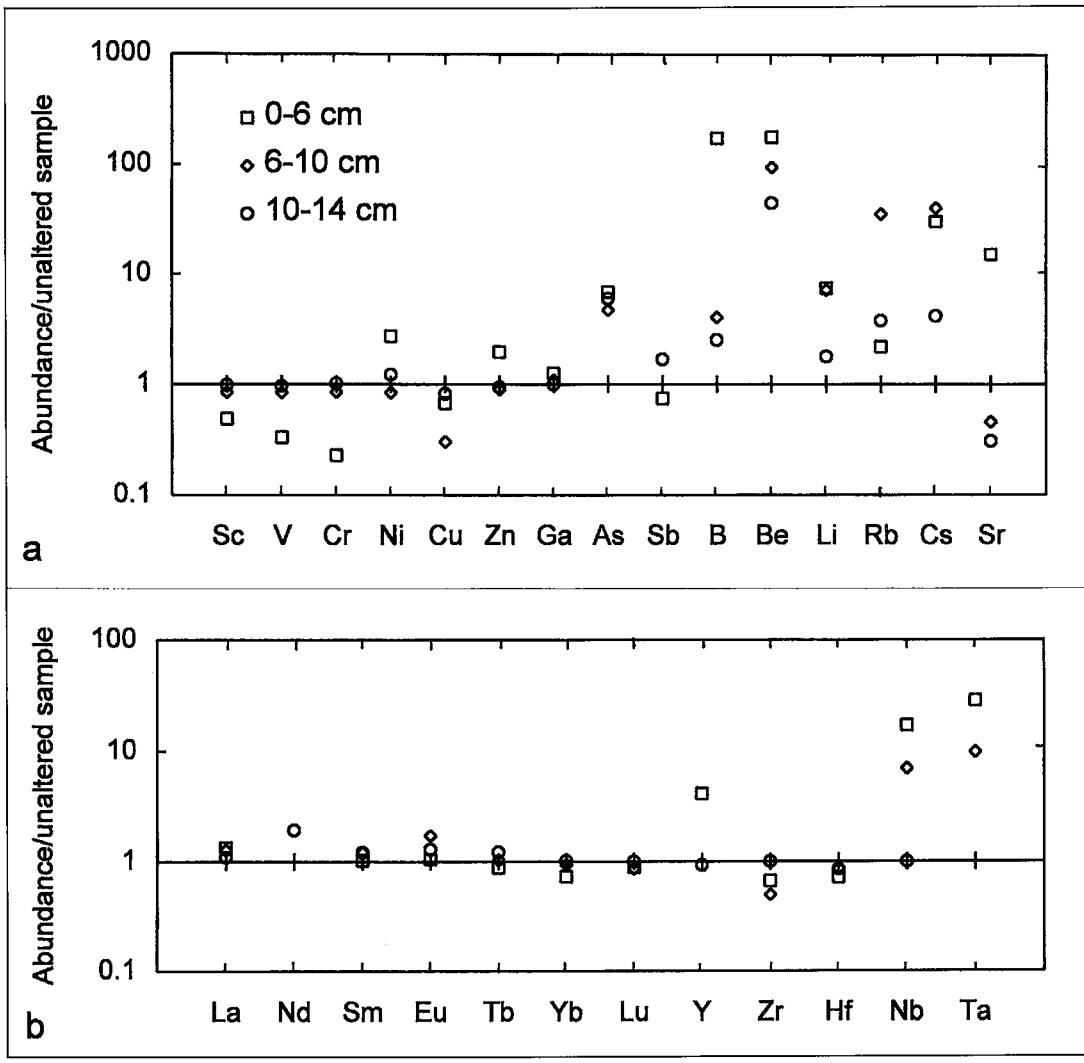

FIG. 15. Trace-element gains and losses within a single traverse of altered amphibolite (sample #17C: Table 8). Compositions are reported at varying distance from a tourmaline–albite vein, and normalized to unaltered amphibolite in local proximity (sample 17F). (a) Transition metals, group-5b elements, light elements, and alkalis. (b) *REE* and *HFSE*. The level of concentration of Se, Ba, Hg, Tl, U, and Th is below the limit of detection.

Temperatures of isotopic equilibrium based on coexisting minerals in pegmatitic systems must be estimated with caution, because widespread open-system conditions, disequilibrium crystallization, subsolidus re-equilibration, and hydrothermal alteration result in small-scale isotopic heterogeneity (Longstaffe 1982). In this study, only mineral pairs have been analyzed (not mineral triplets), such that isotopic equilibrium cannot be rigorously established. The observed quartz–plagioclase fractionation from the granite and a quartz vein are 2.0 and 2.5‰, respectively; these are consistent with equilibrium temperatures of 550 to 500°C, and 400°C, respectively [based on the plagioclase–H_2O fractionation curve of Matsuhisa *et al.* (1979), and the quartz–H_2O fractionation curve of Sharp & Kirchner (1994)].

Plagioclase– muscovite fractionation (O'Neil & Taylor 1969) in a sample of pegmatite is 1.4‰, corresponding to an equilibrium temperature of 450°C. The temperatures derived for the pegmatite and vein compare well with estimates provided by other studies of the magmatic– hydrothermal transition (*cf.* Taylor *et al.* 1979, London 1986b). It is rare that temperatures of isotopic equilibrium in granite predicted from quartz–plagioclase fractionation are >550°C, owing to the easy re-equilibration of plagioclase. The solidus temperature of volatile-rich granitic magma with 1–4 wt% B and F at 1 to 3 kbar is estimated to be 600–650°C [*cf.* experimental work by Wyllie & Tuttle (1961), Manning (1981), and Pichavant (1987)].

Discussion

Although gem-grade aquamarine commonly forms in granitic pegmatite, unusual conditions must occur to produce emerald mineralization. At Khaltaro, the emplacement and crystallization of a small, heterogeneous leucogranite sill and subsequent exsolution of an orthomagmatic fluid resulted in the formation of a beryl-bearing pegmatite–vein system. The orthomagmatic fluid was enriched in H, Si, Al, K, Na, F, Cl, B, Be, Li, Rb, and Cs. Channeling of these fluids along cracks or other permeable zones in the host granite and Cr-bearing amphibolite formed pegmatites and veins composed of quartz, albite, muscovite, and beryl-rich assemblages, including emerald. On the basis of the stable isotope data and phase-equilibrium relationships presented above, the pegmatite – hydrothermal vein system evolved from temperatures of ~650 to 400°C; on the basis of miarolitic cavities in pegmatites and Na^+/K^+ equilibria presented below, the pegmatite – hydrothermal vein system evolved at pressure conditions that were lithostatic and ~0.5 to 2 kbar.

Chemical exchange during amphibolite alteration

Metasomatism of wallrock adjacent to granitic pegmatite is commonly characterized by alkali- and B-metasomatism, characterized by assemblages containing biotite or phlogopite, muscovite, tourmaline, quartz, plagioclase, Li-bearing amphibole (holmquistite), and rare fluorite; chemical mass-transport results in gains of H (as H^+ or H_2O), K, B, Li, Rb, Cs, and F, losses of Mg, Fe, and Ca, and variable changes in Si and Na in the altered wallrock (Jahns 1955, Heinrich 1962, Appleyard 1980, Shearer *et al.* 1984, 1986, Foord *et al.* 1986, London 1986a, Morgan & London 1987, Shearer & Papike 1988, Kretz *et al.* 1989, Laurs & Wise 1991, Martin-Izard *et al.* 1995).

Metasomatism of amphibolite at Khaltaro is characterized by zoned sequential selvages that are symmetrically distributed about an associated pegmatite or vein, and are progressively developed outward in a consistent order without cross-cutting each other. Meyer & Hemley (1967) noted that zoned selvages along veins in epigenetic ore deposits result from synchronous development of the zones during a single metasomatic event. Zoned sequential alteration-induced selvages also are consistent with propagation of a metasomatic front through wallrock of high reactivity but low permeability (Mehnert 1969). Chemical transport in this environment likely occurred by a diffusion–infiltration metasomatism (*cf.* Fletcher & Hofmann 1974, Appleyard 1980), in which dissolved species infiltrate unidirectionally with fluid along a vein but diffuse bidirectionally between a vein and wallrock.

Although the chemical composition of the magmatic fluid cannot be determined precisely, hydrogen ion and alkalis (see below) were likely the important cations, whereas F, Cl, and BO_3 were the important anions. The high F contents of the micas suggest relatively F-rich fluids. Using the method of Munoz & Ludington (1977) and Munoz & Swenson (1981), the F and Cl contents of micas yield calculated fugacity of HCl nearly equal to fugacity of HF [$f(HCl) \approx f(HF)$] for leucogranite and pegmatite at 600°C, and $f(HCl)/f(HF)$ in the range 0.3 to 1 for altered amphibolite and veins at 500°C. Both log $f(H_2O)/f(HF)$ and log $f(H_2O)/f(HCl)$ range from 3 to 4 for all samples. In addition, the F and Cl contents of the biotite and muscovite (F intercept = 0.5 to 1.3; Cl intercept = –2.1 to –3.9) are similar to those in F-rich porphyry Mo deposits, but have a much greater F/Cl ratio than Cl-rich porphyry Cu deposits (Munoz 1984). We conclude that F and Cl contents were similar in the orthomagmatic fluids; the following discussion models cation transport by F-species.

The reaction below describes the mineralogical changes accompanying alteration of the amphibolite caused by fluids derived from the pegmatite – hydrothermal vein system. The principal mechanism of reaction is one of hydrogen ion metasomatism (or hydrolytic alteration), with lesser alkali metasomatism. The reaction written is simplified for the case of zoisite amphibolite, with hornblende and actinolite components used to approximate the overall composition of the amphibole. Garnet is omitted, since it generally occurs in sparse amounts, and beryl is omitted because it is generally absent from the metasomatized amphibolite. An analogous, but entirely equivalent reaction can also be written for the plagioclase amphibolite, by substituting anorthite for zoisite. In that reaction, the anorthite component of plagioclase is largely consumed, but the albite component is relatively stable, so that the relict plagioclase in the metasomatic assemblages is sodic (An_{17}). In the relatively high-temperature environment, hydrogen ion and other cations in the fluids are largely associated with F, Cl, and BO_3, as written. Therefore,

fluids exsolved from the pegmatite-forming leucogranitic magma are only weakly acidic and are buffered by the assemblage K-feldspar – quartz – albite – muscovite. As the fluids traverse along the veins and diffuse into the wallrocks, they cool, and the acids dissociate to produce the hydrolytic alteration observed. Note that these wallrock reactions buffer the fluid pH at slightly acidic values (*e.g.*, assemblage albite–biotite).

$$2Ca_2(Mg,Fe)_4Al(Si_7AlO_{22})(OH)_2 \cdot Ca_2(Mg,Fe)_5Si_8O_{22}(OH)_2 +$$
hornblende actinolite
$$Ca_2Al_3(Si_3O_{12})(OH) +$$
zoisite
$$9HF_{(aq)} + 3KF_{(aq)} + 2AlF_{3(aq)} + NaF_{(aq)} + 3H_3(BO_3)_{(aq)} =$$
$$3K(Mg,Fe)_3(AlSi_3O_{10})(OH)_2 +$$
biotite
$$Na(Mg,Fe)_3Al_6B_3Si_6O_{27}(OH)_3F +$$
tourmaline
$$8CaF_2 + (Mg,Fe)F_{2(aq)} + 10SiO_{2(aq)} + 8H_2O.$$
fluorite water

The reaction is consistent with several of the major-element gains and losses measured in the metasomatized amphibolite. Whole-rock analyses and petrographic examination suggest addition of K, H, F, B, Li, Rb, Cs, Be, Ta, Nb, As, Y, and Sr, and removal of Si, Mg, Ca, Fe, Cr, V, and Sc from the amphibolite (Fig. 12). Substantial enrichment of K, Rb, and Cs corresponds to addition of biotite in the alteration assemblages, and small gains of H_2O are associated with biotite replacement of amphibole. Enrichment of F in the inner and intermediate alteration-zones correlates with the presence of fluorite, as well as high F contents of metasomatic biotite, muscovite, and tourmaline. The inner Biotite – Tourmaline – Fluorite zone locally shows slight gains in Al and Na, which correlate with the presence of tourmaline and albite, but in other cases, it shows slight losses (Fig. 14). Some variation of Al and Na may be due to original compositional heterogeneity in the amphibolite. In the case of minor gains in Al and Na in the inner zone, these elements were probably supplied in small amounts by magmatic fluids (see below). The detected loss of Si from the inner biotite-rich alteration-zones suggests that Si was excluded from the relatively Si-poor minerals in these assemblages. Excess Si released by the conversion of hornblende to biotite was locally precipitated as quartz, and also apparently moved out of the wallrock into the pegmatite–vein system. The (Mg, Fe) and Ca released from the amphibolite during alteration are likely incorporated into tourmaline and fluorite, respectively, in the pegmatites and veins. The Cr released from the alteration of amphibole and zoisite in the amphibolite diffused into the pegmatite–vein system, where it was preferentially incorporated into beryl near the contact. The presence of emerald near the contact indicates that metasomatism of the amphibolite and release of Cr occurred during the initial stages of crystallization of the pegmatite–vein system.

Relations between K- and Na-metasomatism

The Na-metasomatism (albitization) of the pegmatites and leucogranite, and presence of albite-rich veins at Khaltaro, are similar to worldwide associations of albitization with rare metal-enriched (Sn, W, Ta, Nb, Li, Mo, F) granites (*e.g.*, Schwartz & Surjono 1990). K-feldspar is rare in the pegmatites and veins at Khaltaro and was noted in only one pegmatite (Fig. 3: unit Pkpb). Albitization of the leucogranite sill is local and apparently related to the same fluid channels associated with albitized pegmatites and veins. Albitization of pegmatite simply by a cooling orthomagmatic fluid is not expected because the a_{Na^+}/a_{K^+} of a magmatic alkali chloride fluid is fixed by equilibrium with albite + K-feldspar, and increases with decreasing temperature (Orville 1963, Lagache 1984); this relationship predicts that a cooling alkali chloride magmatic fluid would yield K-feldspar replacement of albite, and not the observed albitization. In contrast, studies of alkali fluoride – feldspar equilibria indicate that between 0.5 and 2 kbar, the ratio a_{Na^+}/a_{K^+} of fluid decreases as temperature decreases from 600 to 450°C (Doherty 1990), so that cooling alkali fluoride fluids would produce Na-metasomatism, resulting in albitization of K-feldspar. At pressures of 2 kbar and above, the alkali fluoride system is similar to the alkali chloride system (Barton & Frantz 1983, Doherty 1990); thus, the inferred low pressures at Khaltaro are consistent with F-rich sodium metasomatism. Addition of moderate amounts of F, B, and P to felsic melts shifts the H_2O-saturated minima toward albite away from K-feldspar and quartz (*e.g.*, London 1987), which would yield magmatic aqueous fluids with higher Na^+/K^+ values and therefore accentuate potential sodium metasomatism.

Albitization of the pegmatites and veins may well have been augmented by potassium metasomatism of the amphibolite wallrocks. During wallrock alteration, large amounts of K entered the amphibolite, driven by diffusion along a geochemical gradient. The Na remained within the pegmatite–vein system, which initially had a fluid Na:K molar ratio of approximately 10:1, based on lack of significant addition of Na to the altered amphibolite. With increasing loss of K into the amphibolite, the a_{Na^+}/a_{K^+} ratio increased in the pegmatite and veins, causing the fluid to be out of equilibrium with K-feldspar. Equilibrium a_{Na^+}/a_{K^+} in the pegmatite and vein system was attained by conversion of K-feldspar to albite by the reaction: K-feldspar + Na^+ = Albite + K^+. We observe albitization textures in pegmatite that include partial replacement of relict K-feldspar by albite and by fine-grained intergrowths of albite and muscovite.

Factors affecting emerald mineralization and Be-transport

Emerald mineralization due to metasomatism associated with F-rich granitic pegmatite – hydrothermal vein systems such as Khaltaro is affected by physicochemical conditions of the Cr-bearing host rock. The chemical reactivity and permeability of the host rock determine whether emerald forms within the pegmatite or the altered host-rock. Fractured or schistose ultramafic wallrock containing an abundance of sheet silicates (such as talc or micas) is permeable and reactive to Be-bearing hydrothermal solutions. Since Cr is relatively immobile under moderate- to high-temperature hydrothermal conditions inferred for pegmatite–vein systems, economically important emerald deposits form where Be is transported into Cr-bearing host rock. Indeed, emerald deposits worldwide form in ultramafic schists that are intruded and metasomatized by pegmatite or hydrothermal veins. Complexes of Be^{2+} with fluoride, hydroxide, carbonate, and chloride, as well as mixed ligands, have been proposed for transport of Be under low- to high-temperature conditions (*e.g.*, Govorov & Stunzhas 1963, Mesmer & Baes 1969, Brown *et al.* 1983, Wood 1992). At Khaltaro, Be-fluoride complexes were likely dominant, as suggested by inclusions of F-rich biotite within emerald and the close association of emerald with veins containing F-bearing tourmaline and fluorite. Be-fluoride complexes become unstable when a_{F^-} decreases, which may be caused by precipitation of fluorite or topaz (Wood 1992). At Khaltaro, fluorite precipitation by the reaction $Ca^{2+} + 2F^- = CaF_2$ governs a_{F^-}; topaz is absent. Emerald mineralization is commonly associated with fluorite at or near the pegmatite or vein contacts, where high $a_{Ca^{2+}}$ derived from metasomatism of amphibolite (9 to 17 wt% CaO: Tables 2 and 9; Laurs 1995) is expected to cause beryl precipitation from fluoride complexes. The amount of emerald mineralization within the pegmatite or veins is limited by the availability and transport of Cr from the amphibolite. Although Cr is relatively immobile during metamorphism (Sánchez-Vizcaíno *et al.* 1995), mobility is enhanced in the presence of hydrothermal fluids (Treloar 1987), such as those derived from the pegmatite–vein system at Khaltaro.

Tectonic implications

Emerald mineralization related to the Cenozoic Himalayan collision occurred in two tectonic settings in Pakistan. Emerald with tourmaline and chromian muscovite ($^{40}Ar/^{39}Ar$ age: 23 Ma) occurs in quartz–dolomite veins cutting talc–carbonate schist alteration of ophiolitic *mélange* along the MMT suture at Mingora, Swat (200 km southwest of Khaltaro); its formation was synchronous with emplacement of the nearby Malakand leucogranite (Dilles *et al.* 1994, Arif *et al.* 1996). The Khaltaro deposit represents a younger event that is apparently also related to leucogranite [Jutial: Rb–Sr muscovite ~500–550°C cooling age of 6.5 Ma: George *et al.* (1993)] and pegmatite emplacement (muscovite $^{40}Ar/^{39}Ar$ age of 9.13 ± 0.04 Ma, this study). George *et al.* (1993) reported ages of metamorphism of nearby rocks of 25 to 16 Ma for hornblende ($^{40}Ar/^{39}Ar$ cooling age through 550°C isotherm) and ~28 to 24 Ma for muscovite (Rb–Sr). Although these ages may indicate the timing of peak Cenozoic metamorphism in the Haramosh massif, grades at Khaltaro apparently did not reach the amphibolite facies during the Cenozoic, as indicated by the Paleozoic or older $^{40}Ar/^{39}Ar$ age data for hornblende. Metamorphic muscovite (closure: 325°C) yields a disturbed $^{40}Ar/^{39}Ar$ spectrum of about 9 to 10 Ma, identical to the age of muscovite in cross-cutting beryl-bearing pegmatite. Thus, the wallrocks must have been at temperatures between 325 and 550°C when the Khaltaro pegmatite–vein system was emplaced between ~30 and 10 Ma. The data presented above suggest that leucogranites and pegmatites crystallized at 650 to 600°C, and the vein, emerald mineralization, and wallrock alteration proceeded between ~550 and 400°C at <2 kbar pressure. The presence of sharp intrusive contacts of pegmatites and either weak or no deformation in pegmatites at Khaltaro is similar to what is found in other gem-bearing pegmatites in the Haramosh massif (*e.g.*, Kazmi *et al.* 1985, Kazmi & O'Donoghue 1990) and suggests that these pegmatites were emplaced after peak Himalayan metamorphism, when wallrocks were relatively cool and shallow (~350–400°C, 1–2 kbar) and could fracture in brittle fashion. These requisite conditions formed diachronously across the Nanga Parbat – Haramosh massif, from >9 Ma in the Khaltaro area to ages as young as 1 Ma farther to the south (Zeitler & Chamberlain 1991, Zeitler *et al.* 1993), which suggests earlier uplift of the northwestern Haramosh massif.

Conclusions

At Khaltaro, emerald forms principally within hydrothermal quartz veins and tourmaline–albite veins, which cut amphibolite and are associated with and cross-cut a small heterogeneous sill of Himalayan leucogranite of probable Tertiary age. Emerald also sparingly forms within bodies of albite-rich pegmatite and albitized leucogranite adjacent to amphibolite, and rarely within altered amphibolite along vein contacts. The color of the emerald is due to trace amounts of Cr and Fe. The Cr_2O_3 and $Fe_2O_3{}^T$ contents decrease systematically from emerald (>0.20 and 0.54–0.89 wt%, respectively), to pale blue beryl (≤0.07, 0.10–0.63), to colorless beryl (<0.07, 0.07–0.28). The Cr and Fe are derived from alteration of the

amphibolite wallrocks, principally as a result of hydrogen ion metasomatism by magmatic fluids derived from the pegmatite-forming leucogranitic magma. The amphibolite was altered to assemblages containing biotite, sodic plagioclase and fluorite, with local tourmaline, muscovite, quartz, and rare beryl in symmetrically zoned selvages. Metasomatism of the amphibolite has added K, H, F, B, Li, Rb, Cs, Be, Ta, Nb, As, Y, and Sr, and removed Si, Mg, Ca, Fe, Cr, V, and Sc. Alteration of hornblende and zoisite released Cr, which was incorporated into exomorphic biotite and tourmaline, and also diffused through stagnant pore fluid into the margins of the pegmatite–vein system, where preferential incorporation into beryl produced emerald coloration. The anions in the magmatic fluids were dominated by subequal amounts of F and Cl, as determined from F-rich mica compositions, with important BO_3, and therefore fluoride complexes likely transported much of the beryllium ion, hydrogen ion, and other cations within the pegmatite–vein system. Solutions entering the amphibolite caused alteration that liberated Ca and precipitated fluorite, which may have caused destabilization of Be-fluoride complexes to form beryl. Temperatures inferred from granite melting experiments suggest that the leucogranitic magma crystallized at 600 to 650°C, and those derived from isotopic fractionation suggest that the pegmatite–vein system, amphibolite alteration, and emerald mineralization occurred between 550 and 400°C. Pressures were <3 kbar based on miarolitic cavities in pegmatites, but are likely restricted to 0.5 to 2 kbar if albitization is related to alkali fluoride fluids. Both cooling of alkali fluoride fluids and preferential extraction of K during wallrock alteration may have caused sodium metasomatism of pegmatites and veins.

Acknowledgements

The Geological Survey of Pakistan (GSP) provided logistical support in the field and use of laboratory facilities. We thank S.H. Gauhar and A.B. Kausar of GSP for coordination of logistics, and Y. Warraich of GSP for assistance with fieldwork. Dr. Eugene E. Foord provided inspiration and enthusiasm to one of us (B.L.) during field excursions to gem-bearing pegmatites in San Diego County, California, and tentatively identified a sample of ralstonite from Khaltaro. Drs. Ali H. Kazmi and Nasir Ali Bhatti (Managing Director of Gemstone Corporation) provided helpful information and advice in Pakistan. INAA analyses at the OSU Radiation Center were provided under the Reactor Use Sharing Program. Electron-microprobe analyses were supported by the OSU College of Science and College of Oceanic and Atmospheric Sciences, assisted by R. Nielsen. D. Reinert drafted Figures 1–4 and photographed specimens. This study was funded by the OSU Department of Geosciences Ore Geology Fund, Sigma Xi and OSU graduate research grants (to B.L.), and National Science Foundation grant INT-8609914 (to R.D. Lawrence). This manuscript benefitted from constructive reviews by R.F. Martin, R.D. Lawrence, and an anonymous referee.

References

Anders, E. & Ebihara, M. (1982): Solar-system abundances of the elements. *Geochim. Cosmochim. Acta* **46**, 2363-2380.

Appleyard, E.C. (1980): Mass balance computations in metasomatism: metagabbro/nepheline syenite pegmatite interaction in northern Norway. *Contrib. Mineral. Petrol* **73**, 131-144.

Arif, M., Fallick, A.E. & Moon, C.J. (1996) The genesis of emeralds and their host rocks from Swat, northwestern Pakistan: a stable isotope investigation. *Mineral. Deposita* **31**, 255-268.

Aurisicchio, C., Fioravanti, G., Grubessi, O. & Zanazzi, P.F. (1988): Reappraisal of the crystal chemistry of beryl. *Am. Mineral.* **73**, 826-837.

Bank, H. (1985): New emeralds findings in Afghanistan and in Pakistan. *In* Diamond and Precious Stone Exchange Idar-Oberstein. *Call Idar-Oberstein, Market Rep.* **4/85**, 83-84.

Barton, M.D. & Frantz, J.D. (1983): Exchange equilibria of alkali feldspars with fluorine-bearing fluids. *Carnegie Inst. Wash. Yearbook* **82**, 377-381.

Beus, A.A. (1962): *Beryllium: Evaluation of Deposits During Prospecting and Exploratory Work.* W.H. Freeman & Co., San Francisco, California.

Bottinga, Y. & Javoy, M. (1973): Comments on oxygen isotope geothermometry. *Earth Planet. Sci. Lett.* **20**, 250-265.

Brown, P.L., Ellis, J. & Sylva, R.N. (1983): The hydrolysis of metal ions. 7. Beryllium (II). *J. Chem. Soc., Dalton Trans.*, 2001-2004.

Butler, R.W.H., George, M., Harris, N.B.W., Jones, C., Prior, D.J., Treloar, P.J. & Wheeler, J. (1992): Geology of the northern part of the Nanga Parbat massif, northern Pakistan, and its implications for Himalayan tectonics. *J. Geol. Soc. London* **149**, 557-567.

_____ & Prior, D.J. (1988): Anatomy of a continental subduction zone: the Main Mantle thrust in northern Pakistan. *Geol. Rundsch.* **77**, 239-255.

Coward, M.P., Butler, R.W.H., Chambers, A.F., Graham, R.H., Izzat, C.N., Khan, M.A., Knipe, R.J., Prior, D.J., Treloar, P.J. & Williams, M.P. (1988): Folding and imbrication of the Indian crust during Himalayan collision. *Phil. Trans., R. Soc. London* **A326**, 89-116.

DALRYMPLE, G.B., ALEXANDER, E.C., JR., LANPHERE, M.A. & KRAKER, G.P. (1981): Irradiation of samples for $^{40}Ar/^{39}Ar$ dating using the Geological Survey TRIGA reactor. *U.S. Geol. Surv., Prof. Pap.* **1176**.

DEER, W.A., HOWIE, R.A. & ZUSSMAN, J. (1992): *An Introduction to the Rock-Forming Minerals* (second ed.). Longman, London, U.K.

DILLES, J.H., SNEE, L.W., & LAURS, B.M. (1994): Geology, Ar–Ar age, and stable isotope geochemistry of suture-related emerald mineralization, Swat, Pakistan Himalayas. *Geol. Soc. Am., Abstr. Program* **26**(7), 311.

DOHERTY, S.B. (1990): *An Experimental Investigation of Supercritical Alkali Halide – Mineral Exchange Equilibria.* M.S. thesis, Univ. of California, Los Angeles, California.

FALLICK, A.E. & BARROS, J.G. (1987): A stable-isotope investigation into the origin of beryl and emerald from the Porangatu deposits, Goias State, Brazil. *Chem. Geol.* **66**, 293-300.

FERRY, J.M. & SPEAR, F.S. (1978): Experimental calibration of the partitioning of Fe and Mg between biotite and garnet. *Contrib. Mineral. Petrol.* **66**, 113-117.

FLETCHER, R.P. & HOFMANN, A.W. (1974): Simple models of diffusion and combined diffusion-infiltration metasomatism. *In* Geochemical Transport and Kinetics (A.W. Hofmann, B.J. Giletti, H.S. Yoder, Jr. & R.A. Yund, eds.). *Carnegie Inst. Wash., Publ.* **634**, 243-259.

FOORD, E.E., STARKEY, H.C. & TAGGART, J.E., JR. (1986): Mineralogy and paragenesis of "pocket" clays and associated minerals in complex granitic pegmatites, San Diego County, California. *Am. Mineral.* **71**, 428-439.

GARSTONE, J.D. (1981): The geological setting and origin of emerald deposits at Menzies, Western Australia. *J. Royal Soc. West. Aust.* **64**(2), 53-64.

GEORGE, M.T., HARRIS, N.B.W. & BUTLER, R.W.H. (1993): The tectonic implications of contrasting granite magmatism between the Kohistan island arc and the Nanga Parbat – Haramosh massif, Pakistan Himalaya. *In* Himalayan Tectonics (P.J. Treloar & M.P. Searle, eds.). *Geol. Soc., Spec. Publ.* **74**, 173-191.

GOVOROV, I.N. & STUNZHAS, A.A. (1963): Mode of transport of beryllium in alkali metasomatism. *Geochem. Int.* **4**, 402-409.

GRESENS, R.L. (1967): Composition–volume relationships of metasomatism. *Chem. Geol.* **2**, 47-65.

GRINBERG, A.A. (1951): *Introduction to the Chemistry of Complex Compounds.* 2-e izd. Goskhimizdat, Moscow, Russia (in Russ.).

GROMET, L.P., DYMEK, R.F., HASKIN, L.A. & KOROTEV, R.L. (1984): The "North American Shale Composite": its compilation, major and trace element characteristics. *Geochim. Cosmochim. Acta* **48**, 2469-2482.

GRUNDMANN, G. & MORTEANI, G. (1989): Emerald mineralization during regional metamorphism: the Habachtal (Austria) and Leydsdorp (Transvaal, South Africa) deposits. *Econ. Geol.* **84**, 1835-1849.

HAMMARSTROM, J.M. (1989): Mineral chemistry of emeralds and some associated minerals from Pakistan and Afghanistan: an electron microprobe study. *In* Emeralds of Pakistan: Geology, Gemology, and Genesis (A.H. Kazmi & L.W. Snee, eds.). Van Nostrand Reinhold, New York, N.Y. (125-150).

HARRIS, N.B.W. & INGER, S. (1992): Trace element modeling of pelite-derived granites. *Contrib. Mineral. Petrol.* **110**, 46-56.

———, ——— & MASSEY, J. (1993): The role of fluids in the formation of High Himalayan leucogranites. *In* Himalayan Tectonics (P.J. Treloar & M.P. Searle, eds.). *Geol. Soc., Spec. Publ.* **74**, 391-400.

———, PEARCE, J.A. & TINDLE, A.G. (1986): Geochemical characteristics of collision-zone magmatism. *In* Collision Tectonics (M.P. Coward & A.C. Ries, eds.). *Geol. Soc., Spec. Publ.* **19**, 67-81.

HEINRICH, E.W. (1962): Pegmatites at Ryrs, Sweden – examples of fluorite exomorphism. *Am. Mineral.* **47**, 924-931.

JAHNS, R.H. (1955): The study of pegmatites. *Econ. Geol., 50th Anniv. Vol.*, 1025-1130.

KAZMI, A.H., ANWAR, J., HUSSAIN, S., KHAN, T. & DAWOOD, H. (1989): Emerald deposits of Pakistan. *In* Emeralds of Pakistan: Geology, Gemology, and Genesis (A.H. Kazmi & L.W. Snee, eds.). Van Nostrand Reinhold, New York, N.Y. (39-74).

——— & O'DONOGHUE, M. (1990): *Gemstones of Pakistan: Geology and Gemmology.* Gemstone Corporation of Pakistan, Peshawar, Pakistan.

———, PETERS, J.J. & OBODDA, H.P. (1985): Gem pegmatites of the Shingus–Dusso area, Gilgit, Pakistan. *Mineral. Rec.* **16**, 393-411.

——— & SNEE, L.W. (1989): Geology of world emerald deposits: a brief review. *In* Emeralds of Pakistan: Geology, Gemology, and Genesis (A.H. Kazmi & L.W. Snee, eds.). Van Nostrand Reinhold, New York, N.Y. (165-236).

KHAN, I.A. & AZIZ, K. (1985): A brief note on the beryl and emerald-bearing pegmatites of Khaltaro area, Gilgit. Gemstone Corporation of Pakistan, Peshawar, unpubl. report.

KRETZ, R. (1983): Symbols for rock-forming minerals. *Am. Mineral.* **68**, 277-279.

———, HARTREE, R. & JONES, P. (1989): Metasomatic crystallization of muscovite in granite and tourmaline in schist related to pegmatite emplacement near Yellowknife, Canada. *Contrib. Mineral. Petrol.* **102**, 191-204.

LAGACHE, M. (1984): The exchange equilibrium distribution of alkali and alkaline-earth elements between feldspars and hydrothermal solutions. *In* Feldspars and Feldspathoids (W.L. Brown, ed.). *NATO Adv. Study Inst. Ser.* **C 137**, 247-279. Kluwer, Dordrecht, The Netherlands.

LAURS, B.M. (1995): *Emerald Mineralization and Amphibolite Wall-Rock Alteration at the Khaltaro Pegmatite-Hydrothermal Vein System, Haramosh Mountains, Northern Pakistan.* M.S. thesis, Oregon State Univ., Corvallis, Oregon.

_____ & WISE, W.S. (1991): The metasomatic effects of the emplacement and crystallization of the Himalaya pegmatite–aplite dike on gabbronorite wallrock, San Diego County, California. *Discovery: University of California, Santa Barbara, Journal of Undergraduate Research* **14**, 100-138.

LAWRENCE, R.D. & GHAURI, A.A.K. (1983): Evidence of active faulting in the Chilas District, northern Pakistan. *Geol. Bull., Univ. Peshawar* **16**, 185-186.

LEAKE, B.E. (1978): Nomenclature of amphiboles. *Am. Mineral.* **63**, 1023-1052.

LONDON, D. (1986a): Holmquistite as a guide to pegmatitic rare-metal deposits. *Econ. Geol.* **81**, 704-712.

_____ (1986b): Formation of tourmaline-rich gem pockets in miarolitic pegmatites. *Am. Mineral.* **71**, 396-405.

_____ (1987): Internal differentiation of rare-element pegmatites: effects of boron, phosphorus, and fluorine. *Geochim. Cosmochim. Acta* **51**, 403-420.

LONGSTAFFE, F.J. (1982): Stable isotopes in the study of granitic pegmatites and related rocks. *In* Granitic Pegmatites in Science and Industry (P. Černý, ed.). *Mineral. Assoc. Can., Short-Course Handbook* **8**, 373-404.

MADIN, I.P. (1986): *Structure and Neotectonics of the Northwestern Nanga Parbat – Haramosh Massif.* M.S. thesis, Oregon State Univ., Corvallis, Oregon.

_____, LAWRENCE, R.D. & UR-REHMAN, S. (1989): The northwestern Nanga Parbat – Haramosh massif: evidence for crustal uplift at the northwestern corner of the Indian craton. *In* Tectonics of the Western Himalayas (L.L. Malinconico & R.J. Lillie, eds.). *Geol. Soc. Am., Spec. Pap.* **232**, 169-182.

MANNING, D.A.C. (1981): The effect of fluorine on liquidus phase relationships in the system Qz–Ab–Or with excess water at 1 kb. *Contrib. Mineral. Petrol.* **76**, 206-215.

MARIANO, A.N. (1987a): Geochemical characterization of mineral deposits – Pakistan. *United Nations Department of Technical Cooperation for Development* (unpubl.).

_____ (1987b): Gemstone exploration and beneficiation. *United Nations/DTCD Project* **PAK/85-001** (unpubl.).

MARTIN-IZARD, A., PANIAGUA, A., MOREIRAS, D., ACEVEDO, R.D. & MARCOS-PASCUAL, C. (1995): Metasomatism at a granitic pegmatite – dunite contact in Galicia: the Franqueira occurrence of chrysoberyl (alexandrite), emerald, and phenakite. *Can. Mineral.* **33**, 775-792.

MATSUHISA, Y., GOLDSMITH, J.R. & CLAYTON, R.N. (1979): Oxygen isotopic fractionation in the system quartz – albite – anorthite – water. *Geochim. Cosmochim. Acta* **43**, 1131-1140.

MEHNERT, K.R. (1969): Composition and abundance of common metamorphic rock types. *In* Handbook of Geochemistry **1** (K.H. Wedepohl, ed.). Springer-Verlag, Berlin, Germany (272-296).

MESMER, R.E. & BAES, C.F., JR. (1969): Fluorine complexes of beryllium (II) in aqueous media. *Inorg. Chem.* **8**, 618-626.

MEYER, C. & HEMLEY, J.J. (1967): Wall rock alteration. *In* Geochemistry of Hydrothermal Ore Deposits (H.L. Barnes, ed.). Holt, Rinehart & Winston, New York, N.Y. (166-232).

MORGAN, G.B., VI & LONDON, D. (1987): Alteration of amphibolitic wallrocks around the Tanco rare-element pegmatite, Bernic Lake, Manitoba. *Am. Mineral.* **72**, 1097-1121.

MUNOZ, J.L. (1984): F–OH and Cl–OH exchange in micas with applications to hydrothermal ore deposits. *In* Micas (S.W. Bailey, ed.). *Rev. Mineral.* **13**, 469-493.

_____ & LUDINGTON, S.D. (1977): Fluoride–hydroxyl exchange in synthetic muscovite and its application to muscovite–biotite assemblages. *Am. Mineral.* **62**, 304-308.

_____ & SWENSON, A. (1981): Chloride–hydroxyl exchange in biotite and estimation of relative HCl/HF activities in hydrothermal fluids. *Econ. Geol.* **76**, 2212-2221.

O'NEIL, J.R. (1986): Theoretical and experimental aspects of isotopic fractionation. *In* Stable Isotopes in High Temperature Geological Processes (J.W. Valley, H.P. Taylor, Jr. & J.R. O'Neil, eds.). *Rev. Mineral.* **16**, 1-40.

_____ & TAYLOR, H.P., JR. (1969): Oxygen isotope equilibrium between muscovite and water. *J. Geophys. Res.* **74**, 6012-6022.

ORVILLE, P.M. (1963): Alkali ion exchange between vapor and feldspar phases. *Am. J. Sci.* **261**, 201-237.

PEARCE, J.A. & PARKINSON, I.J. (1993): Trace element models for mantle melting: applications to volcanic arc petrogenesis. *In* Magmatic Processes and Plate Tectonics (H.M. Prichard, T. Alabaster, N.B.W. Harris & C.R. Neary, eds.). *Geol. Soc., Spec. Publ.* **76**, 373-403.

PICHAVANT, M. (1987): Effects of B and H_2O on liquidus phase relations in the haplogranite system at 1 kbar. *Am. Mineral.* **72**, 1056-1070.

POGNANTE, U., BENNA, P. & LE FORT, P. (1993): High-pressure metamorphism in the High Himalayan Crystallines of the Stak valley, northeastern Nanga Parbat – Haramosh syntaxis, Pakistan Himalaya. *In* Himalayan Tectonics (P.J. Treloar & M.P. Searle, eds.). *Geol. Soc., Spec. Publ.* **74**, 161-172.

RODDICK, J.C. (1983): High precision intercalibration of ^{40}Ar–^{39}Ar standards. *Geochim. Cosmochim. Acta* **47**, 887-898.

SAMOILOVICH, M.I., TSINOBER, L.I. & DUNIN-BARKOVSKII, R.L. (1971): Nature of the coloring in iron-containing beryl. *Sov. Phys. Crystallogr.* **16**, 147-150.

SAMSON, S.D. & ALEXANDER, E.C., JR. (1987): Calibration of the interlaboratory ^{40}Ar–^{39}Ar dating standard, MMhb–1. *Chem. Geol.* **66**, 27-34.

SÁNCHEZ-VIZCAÍNO, V.L., FRANZ, G. & GÓMEZ-PUGNAIRE, M.T. (1995): The behavior of Cr during metamorphism of carbonate rocks from the Nevado–Filabride complex, Betic Cordilleras, Spain. *Can. Mineral.* **33**, 85-104.

SCAILLET, B., FRANCE-LANORD, C. & LE FORT, P. (1990): Bradinath–Gangotri plutons (Garhwal, India): petrological and geochemical evidence for fractionation processes in a High Himalayan leucogranite. *J. Volc. Geotherm. Res.* **44**, 163-188.

SCHWARTZ, M.O. & SURJONO (1990): Greisenization and albitization at the Tikus tin–tungsten deposit, Belitung, Indonesia. *Econ. Geol.* **85**, 691-713.

SHARP, Z.D. (1990): A laser-based microanalytical method for the *in situ* determination of oxygen isotope ratios in silicates and oxides. *Geochim. Cosmochim. Acta* **54**, 1353-1357.

_____ & KIRCHNER, D.L. (1994): Quartz–calcite oxygen isotope thermometry: a calibration based on natural isotopic variations. *Geochim. Cosmochim. Acta* **58**, 4491-4501.

SHEARER, C.K. & PAPIKE, J.J. (1988): Pegmatite–wallrock interaction: holmquistite-bearing amphibolite, Edison pegmatite, Black Hills, South Dakota. *Am. Mineral.* **73**, 324-337.

_____, _____, SIMON, S.B., LAUL, J.C. & CHRISTIAN, R.P. (1984): Pegmatite/wallrock interactions, Black Hills, South Dakota: progressive boron metasomatism adjacent to the Tip Top pegmatite. *Geochim. Cosmochim. Acta* **48**, 2564-2579.

_____, _____, _____ & LAUL, J.C. (1986): Pegmatite–wallrock interactions, Black Hills, South Dakota: interaction between pegmatite-derived fluids and quartz – mica schist wallrock. *Am. Mineral.* **71**, 518-539.

SINKANKAS, J. (1989): *Emerald and other Beryls.* Geoscience Press, Prescott, Arizona.

SLIWA, A.S. & NGULUWE, C.A. (1984): Geological setting of Zambian emerald deposits. *Precambr. Res.* **25**, 213-228.

SMITH, H.A., CHAMBERLAIN, C.P. & ZEITLER, P.K. (1992): Documentation of Neogene regional metamorphism in the Himalayas of Pakistan using U–Pb in monazite. *Earth Planet. Sci. Lett.* **113**, 93-105.

SNEE, L.W., FOORD, E.E., HILL, B. & CARTER, S.J. (1989): Regional chemical differences among emeralds and host rocks of Pakistan and Afghanistan: implications for the origin of emerald. *In* Emeralds of Pakistan: Geology, Gemology, and Genesis (A.H. Kazmi & L.W. Snee, eds.). Van Nostrand Reinhold, New York, N.Y. (93-124).

_____, LUND, K., SUTTER, J.F., BALCER, D.E. & EVANS, K.V. (1995): An $^{40}Ar/^{39}Ar$ chronicle of the tectonic development of the Salmon River suture zone, western Idaho. *U.S. Geol. Surv., Prof. Pap.* **1438**, 359-414.

_____, SUTTER, J.F. & KELLY, W.C. (1988): Thermochronology of economic mineral deposits – dating the stages of mineralization at Panasqueira, Portugal, by high-precision $^{40}Ar/^{39}Ar$ age-spectrum techniques on muscovite. *Econ. Geol.* **83**, 335-354.

SOLOV'YEV, A.T., CHUPROV, V.V. & MOIZHES, I.B. (1967): Geochemistry of fluorine in the alkalic rocks of western Transbaikalia. *Geochem. Int.* **4**, 278-285.

STAATZ, M.H., GRIFFITTS, W.R. & BARNETT, P.R. (1965): Differences in the minor element composition of beryl in various environments. *Am. Mineral.* **50**, 1783-1795.

STEIGER, R.H. & JÄGER, E. (1977): Subcommission on geochronology -convention on the use of decay constants in geo- and cosmo-chronology. *Earth Planet. Sci. Lett.* **36**, 359-362.

STRECKEISEN, A.L. (1976): To each plutonic rock its proper name. *Earth Sci. Rev.* **12**, 1-33.

SUN, SHEN-SU & MCDONOUGH, W.F. (1989): Chemical and isotopic systematics of ocean basalts: implications for mantle composition and processes. *In* Magmatism in the Ocean Basins (A.D. Saunders & M.J. Norry, eds.). *Geol. Soc., Spec. Publ.* **42**, 313-345.

TAYLOR, B.E., FOORD, E.E. & FRIEDRICHSEN, H. (1979): Stable isotope and fluid inclusion studies of gem-bearing granitic pegmatite–aplite dikes, San Diego County, California. *Contrib. Mineral. Petrol.* **68**, 187-205.

TAYLOR, H.P., JR. (1979): Oxygen and hydrogen isotope relationships in hydrothermal mineral deposits. *In* Geochemistry of Hydrothermal Ore Deposits (second edition, H.L. Barnes, ed.). Wiley, New York, N.Y. (236-277).

TRELOAR, P.J. (1987): The Cr-minerals of Outokumpu – their chemistry and significance. *J. Petrol.* **28**, 867-886.

_____, POTTS, G.J., WHEELER, J. & REX, D.C. (1991): Structural evolution and asymmetric uplift of the Nanga Parbat syntaxis, Pakistan Himalaya. *Geol. Rundsch.* **80**, 411-428.

_____, WHEELER, J. & POTTS, G.J. (1994): Metamorphism and melting within the Nanga Parbat syntaxis, Pakistan Himalaya. *Mineral. Mag.* **58A**, 910-911.

VERPLANCK, P.L. (1986): *A Field and Geochemical Study of the Boundary Between the Nanga Parbat – Haramosh Massif and the Ladakh Arc Terrane, Northern Pakistan*, M.S. thesis, Oregon State Univ., Corvallis, Oregon.

WINSLOW, D.M., CHAMBERLAIN, C.P. & ZEITLER, P.K. (1995): Metamorphism and melting of the lithosphere due to rapid denudation, Nanga Parbat Massif, Himalaya. *J. Geol.* **103**, 395-409.

WOOD, D.L. & NASSAU, K. (1968): The characterization of beryl and emerald by visible and infrared absorption spectroscopy. *Am. Mineral.* **53**, 777-800.

WOOD, S.A. (1992): Theoretical prediction of speciation and solubility of beryllium in hydrothermal solution to 300°C at saturated vapor pressure: application to bertrandite/phenakite deposits. *Ore Geol. Rev.* **7**, 249-278.

WYLLIE, P.J. & TUTTLE, O.F. (1961): Experimental investigation of silicate systems containing two volatile components. II. The effects of NH_3 and HF, in addition to H_2O on the melting temperatures of albite and granite. *Am. J. Sci.* **259**, 128-143.

ZEITLER, P.K. (1985): Cooling history of the NW Himalaya, Pakistan. *Tectonics* **4**, 127-151.

_____ & CHAMBERLAIN, C.P. (1991): Petrogenetic and tectonic significance of young leucogranites from the northwestern Himalaya, Pakistan. *Tectonics* **10**, 729-741.

_____, _____ & SMITH, H.C. (1993): Synchronous anatexis, metamorphism, and rapid denudation at Nanga Parbat (Pakistan Himalaya). *Geology* **21**, 347-350.

_____, SUTTER, J.F., WILLIAMS, I.S., ZARTMAN, R. & TAHIRKHELI, R.A.K. (1989): Geochronology and temperature history of the Nanga Parbat – Haramosh Massif, Pakistan. *In* Tectonics of the Western Himalayas (L.L. Malinconico & R.J. Lillie, eds.). *Geol. Soc. Am., Spec. Pap.* **232**, 1-22.

Received September 29, 1995, revised manuscript accepted September 15, 1996.